Drifting Motions of the Adenovirus Receptor CAR and Immobile Integrins Initiate Virus Uncoating and Membrane Lytic Protein Exposure

Burckhardt, C J ; Suomalainen, M ; Schoenenberger, P ; Boucke, K ; Hemmi, S ; Greber, U F

Abstract: Viral particle binding to plasma membrane receptors elicits virus motions, recruits signaling proteins, and triggers membrane bending and fission, finally resulting in endocytic virus uptake. Here we analyze how human adenovirus engages its receptor coxsackievirus adenovirus receptor (CAR) and coreceptor v integrin to move on the plasma membrane. Virus binding to CAR through fiber knobs gave rise to diffusive motions and actomyosin-2-dependent drifts, while integrin-targeted viruses were spatially more confined. Diffusions, drifts, and confined motions were specifically observed with viral particles that were subsequently internalized. CAR-mediated drifts together with integrin binding supported fiber shedding from adenovirus particles, leading to exposure of the membrane-lytic internal virion protein VI and enhanced viral escape from endosomes. Our results show that adenovirus uncoating is initiated at the plasma membrane by CAR drifting motion and binding to immobile integrins.

DOI: https://doi.org/10.1016/j.chom.2011.07.006

Drifting motions of the adenovirus receptor CAR and immobile integrins initiate virus uncoating and membrane lytic protein exposure

Christoph J. Burckhardt (1)(2), Maarit Suomalainen (1), Philipp Schoenenberger (1), Karin Boucke (1), Silvio Hemmi (1) and Urs F. Greber (1)+)

(1) Institute of Molecular Life Science, University of Zürich, Winterthurerstrasse 190, 8057 Zürich, Switzerland

(2) current address: Department of Cell Biology, Harvard Medical School, Boston, Massachusetts 02115, USA

+) Contact information for corresponding author:

Urs F. Greber, email: urs.greber@imls.uzh.ch, Tel: +41 44 635 4841

Keywords:

CAR (Coxsackievirus Adenovirus Receptor); plasma membrane; infection; virus entry; trajectory segmentation; single particle tracking; actin; myosin-2; integrin; membrane penetration; movement; diffusion; surfing; confinement; motions

Running title:

Virus uncoating by cell surface receptor motions

Summary

Viral particle binding to plasma membrane receptors elicits virus motions, recruits signaling proteins, and triggers membrane bending and fission, finally resulting in endocytic virus uptake. Here we analyze how human adenovirus engages its receptor coxsackievirus-adenovirus-receptor (CAR) and co-receptor αv integrin to move on the plasma membrane. Virus binding to CAR through fiber knobs gave rise to diffusive motions, and acto-myosin-2 dependent drifts, while integrin-targeted viruses were spatially more confined. Diffusions, drifts and confined motions were specifically observed with viral particles that were subsequently internalized. CAR-mediated drifts together with integrin binding supported fiber shedding from adenovirus particles, leading to exposure of the membrane-lytic internal virion protein VI and enhanced viral escape from endosomes. Our results show that adenovirus uncoating is initiated at the plasma membrane by CAR drifting motion and binding to immobile integrins.

Highlights

- Diffusion, drifts and confined motions of adenovirus (Ad2) occur prior to endocytosis
- Diffusion and drifts require CAR, drifts are mediated by dynamic actin and myosin-2
- Ad2 targeted to αv integrins in the absence of CAR has reduced drifts and infection
- Drifts and integrin contacts promote Ad2 uncoating and membrane-lytic protein exposure

Introduction

Binding of virus particles to receptors in the plasma membrane elicits virus motions, recruits signaling proteins, and triggers uptake through membrane bending and fission processes (Burckhardt and Greber, 2009; Doherty and McMahon, 2009; Mercer et al., 2010; Mothes et al., 2010). Viral motions on the cell surface support transmission of particles between cells (Sherer et al., 2007), and it has been proposed that they enhance infection by transporting particles to sites competent for signaling and endocytosis (Ewers et al., 2005; Lehmann et al., 2005; Schelhaas et al., 2008). How the motions of particles are coupled to downstream events, such as endocytosis, and how they impact on viral infection mechanisms is, however, unknown.

Adenoviruses cause upper and lower respiratory tract infections, affect the urinary and digestive tracts, and occasionally give rise to epidemic conjunctivitis and death of immune-compromised patients (Hayashi and Hogg, 2007; Hierholzer, 1992). Adenoviruses are non-enveloped particles with 720 hexon subunits arranged as 240 trimers on a pseudo-T=25 icosahedral lattice (Liu et al., 2010; Reddy et al., 2010). Pentameric penton-base proteins are positioned at the vertices and anchor the protruding trimeric fibers. The terminal fiber knobs (FK) bind with high affinity to the type 1 transmembrane protein coxsackievirus adenovirus receptor (CAR, Bergelson et al., 1997; Roelvink et al., 1999). In normal polarized cells, CAR is involved in cell-cell adhesions at the basolateral domain and tight junctions (Coyne and Bergelson, 2005), and also has activation and effector functions by binding to JAML (junction adhesion molecule-like protein) of mucosal γδ T cells (Witherden et al., 2010). Upon stimulation with cytokines, CAR and αv-β3 integrin coreceptors relocate to the apical membrane, and mediate apical infection with Ad2/5 (Lutschg et al., 2011).

Adenoviruses require integrins for infection (reviewed in Stewart and Nemerow, 2007). αv-β3/5 integrins bind to the protruding RGD (arginine-glycine-aspartate) motif in penton-base of human adenovirus type 2 (HAdV2, short Ad2, Chiu et al., 1999; Wickham et al., 1993), and promote dynamin and actin-dependent viral endocytosis (Li et al., 1998; Meier et al., 2002; Wang et al., 1998), and escape from endosomes to the cytosol (Gastaldelli et al., 2008).

Ad2 and the closely related Ad5, undergo identical step-wise uncoating programs during entry. The uncoating starts with release of fibers and penton base and ends with DNA genome delivery to the nucleus (Greber et al., 1993; Nakano et al., 2000). Viral escape from endosomes requires the exposure of the internal capsid protein VI, which has membrane disruption functions *in vitro* (Maier et al., 2010; Wiethoff et al., 2005) and *in vivo* (Moyer et al., 2011). The cues for protein VI activation are, however, unknown. Interestingly, the mutant Ad2-TS1 (TS1), which has a defect in proteolytic processsing of cementing proteins due to a point mutation in the viral protease (Imelli et al., 2009), contains stabilized rings of peripentonal hexons (Perez-Berna et al., 2009), does not release the fibers or penton-base and remains trapped in endosomes and is degraded in lysosomes (Greber et al., 1996). The surface cryo-EM structure of TS1 is identical to wild-type Ad2 (Perez-Berna et al., 2009; Silvestry et al., 2009). This suggests that depending on the mechanical stability of the capsid, cellular cues induce virus uncoating.

Uncoating of non-enveloped viruses is increasingly recognized to require cellular cues. For picornaviruses, such as the poliomyelitis causing poliovirus, certain enteric coxsackieviruses, hepatitis A virus or common cold causing ICAM-1 (intercellular adhesion molecule-1)-tropic rhinoviruses, receptor binding leads to the loss of the internal viral protein (VP) 4 and the extrusion of the membrane active N-terminal peptide of VP1 (Smyth and Martin, 2002). In case of poliovirus, this lowers the transition state energy for the conversion to subviral particles (Tsang et al., 2001). For the invertebrate nodavirus Flock House virus, the acidic endosomal environment triggers the autocatalytic release of a small membrane-

active protein (Odegard et al., 2009), or triggers the cellular cystein protease cathepsin L, which cleaves reovirus capsid proteins yielding membrane active subviral particles (Ebert et al., 2002). Thiol-disulfide oxido-reductases have been shown to isomerize disulfide bonds of simian virus 40 in the ER, thereby unlinking the major capsid protein VP1, and releasing some VP1 proteins (Schelhaas et al., 2007). Here we studied the mechanism, by which human adenovirus (HAdV, short Ad) species C initiates uncoating on the cell surface. We found a dual cue drifting virus receptors (CAR) and confined motions by integrins that trigger the shedding of fibers from the particle and the activation of the internal capsid protein VI. These initial steps in the uncoating program prime the virus for infectious endocytosis and endosomal escape.

Results

Three distinct motions of extracellular human adenovirus type 2 on filopodia and the cell body

To analyze cell surface motions of Ad2, we inoculated human embryonic retinoblast (HER) 911 cells stably expressing eGFP-actin with Atto565 labeled Ad2 (Ad2-atto565), and recorded viral motions on filopodial extensions and the cell body at an acquisition frequency of 25 Hz up to 5 min post addition of viruses (see Suppl. Mov. 1 and 2). Extracellular low pH quenching experiments of FITC-labeled Ad2-atto565 indicated that more than 90% of the viral particles were pH-sensitive. These paticles lost the FITC signal up to 10 min post warming after cold binding, but retained the pH-insensitive Atto565 signal. Thus, the vast majority of viruses were extracellular (Suppl. Fig. S1A). To obtain virus trajectories, images were processed by a single particle tracking algorithm (Sbalzarini and Koumoutsakos, 2005). Visual inspection of virus trajectories revealed that trajectories were of considerable heterogeneity, but contained three distinct motion patterns, which we refer to as diffusion, drifts and confined motions (Fig.

1a, 2c). To automatically extract these patterns from large sets of trajectories we trained a machine learning-based trajectory segmentation algorithm (Helmuth et al., 2007). This algorithm identified the three virus motion patterns at 90-95% accuracy.

To characterize the movements of Ad2-atto565 on L929-CAR cells, we determined the diffusion constant D, the moment scaling spectrum (MSS) slope (Ewers et al., 2005; Helmuth et al., 2007), and the size and duration of the motion patterns (Suppl. Fig. S1B). MSS slopes are a measure for the diffusive behavior, where values below 0.5 indicate confined diffusion, values of 0.5 random walks, and values above 0.5 diffusion with underlying drifts (see also Ewers et al., 2005). A value of 1 would be obtained for a linear trajectory. Characteristically, the confined motions of Ad2-atto565 had diffusion constants between 0.001 and 0.01 $\mu m^2/s$ and MSS slopes around 0.2, while drifts had narrowly distributed D values around 0.005 $\mu m^2/s$ and MSS slopes between 0.2 and 0.7 (Suppl. Fig. S1B, a,d,g,j). The Ad2-atto565 drifts were found to be aligned in a directionality versus distance plot, unlike the confined motions (restricted to areas smaller 0.25 μm^2) or the diffusive motions (covering larger areas), indicating that drifts moved directionally (Suppl. Fig. S1B, b,e,h,k). The durations of drifts were often longer than the confined motions, sometimes up to 50 s (Suppl. Fig. S1B, c,f,i,l). The diffusive motions, on the other hand, were short lived in the range of few seconds, with D values of 0.05 $\mu m^2/s$ and MSS slopes between 0.2 and 0.6. The remaining nonclassified motions (less than 2% of the virus live time at the cell surface) had similar properties as the diffusive motions (Suppl. Fig. S1B, m-o). This shows that the diffusions, drifts and confined motions occupied different but partly overlapping areas in the multiparameter feature space of MSS slope, D, size, directionality and duration. The combination of such features allows the automated detection of motion patterns by machine learning-based trajectory segmentation. With this powerful procedure, we found diffusion, drifts and confined motions of Ad2-atto565 on both filopodia (Fig. 1a, tracks 1-3, Fig. 1b, Suppl. Mov. 1) and the cell body (Fig. 1a, tracks 4, 5, Fig. 1b, Suppl. Mov. 2). In

both instances the drifts had speeds around 10-40 nm/s and lengths up to 2-3 µm (Suppl. Fig. S1C).

Mechanistically, the drifts could be due to passive coupling to a moving matrix, such as an actin or microtubule network, or they could be driven by actin assembly, or directly by a processive motor moving on a cytoskeletal track. Inhibition of actin filament growth by cytochalasin D (cytoD), which binds to the fast growing end of actin and depolymerizes actin filaments, or inhibition of myosin-2 with blebbistatin (Straight et al., 2003) significantly reduced the Ad2-atto565 drifts without affecting diffusion or confined motions (Fig. 1b). The viral drifts on the cell body of human melanoma M21 cells were also inhibited by the actin sequestering drug latrunculin B (data not shown), while depolymerization of microtubules by nocodazole did not reduce drifts in M21 cells (Suppl. Fig. S1C). In fact, nocodazole significantly enhanced the acto-myosin dependent drifts from 7.2 to 10.4%. This is in agreement with previous reports showing that depolymerization of microtubules increases the levels of F-actin by activation of microtubule-associated Rho guanine exchange factors (Danowski, 1989; Krendel et al., 2002), and changes the viscoelastic properties of the cortical acto-myosin network. Together, the data show that adenovirus drifts require an intact and dynamic actin cytoskeleton, and the actin-dependent myosin-2 motor protein, while the diffusive motions and confined motions were independent of actin.

Diffusive motions of adenovirus upstream of endocytosis depend on CAR

To analyze the motion patterns upstream of virus endocytosis, we recorded movies of Ad2-atto565 by total internal reflection fluorescence (TIRF) microscopy on dynamin2-EGFP expressing HER-911 cells at 37°C up to 10 min post binding. Functional analyses have indicated that Ad2 internalization depends on the large GTPase dynamin (Gastaldelli et al., 2008; Meier et al., 2002) as well as on actin (Nakano et al., 2000). Viruses that disappeared from the TIRF view together with a spatially and temporally correlated peak of dynamin2-EGFP intensity (blink)

were selected (for a representative example, see Fig. 2a-c and Suppl. Mov. 3). Dynamin blinks are diagnostic hallmarks for dynamin recruitment to clathrin-coated pits shortly before the pits move away from the plasma membrane (Merrifield et al., 2002; Perrais and Merrifield, 2005). Analysis of 20 events demonstrated that adenovirus disappearance coincided with a peak in dynamin2-EGFP intensity, which lasted for about 30 s (Suppl. Fig. S2). This burst time was identical to dynamin2-EGFP bursts in clathrin-mediated endocytosis of transferrin, vesicular stomatitis virus or sorting nexin 9 regulated dynamin assembly (Cureton et al., 2009; Perrais and Merrifield, 2005; Soulet et al., 2005). Hence, we classified these events as internalizing viruses. The average life-time of the viruses on the cell surface was 322+/-136 s (mean+/-std, n=20), well within the range of biochemical measurements (Gastaldelli et al., 2008; Greber et al., 1993).

Trajectory segmentation revealed that all 3 types of motion occurred prior to internalization (Fig. 2c-d) with a considerable heterogeneity in the sequence of different motion types (Fig 2e). Alignments of the trajectories to the time point of virus attachment on the cell surface showed that about 80% of all viruses were in diffusive motions during the first 15 s after cell binding (Fig. 2f). The fraction of diffusion rapidly decreased to about 40% at 50 s and 15% at 200 s, while drifts and confined motions increased. This suggested that the longer the viruses resided on the plasma membrane, the less likely they were to diffuse.

The trimeric FK is necessary and sufficient to attach the virus particle to CAR (Bergelson et al., 1997; Bewley et al., 1999; Roelvink et al., 1999). We used purified FK (Suppl. Fig. S3, a) to test whether Ad5 FK binding to CAR clusters multiple CAR molecules, and performed fluorescence recovery after photobleaching experiments in L929 cells expressing an N-terminally fused GFP-CAR. We found that FK delayed the recovery of GFP-CAR fluorescence (Suppl. Fig. S3, b,c), consistent with FK clustering multiple GFP-CAR. In addition, we performed single particle tracking of fluorescently labeled FK-atto565 that showed diffusive behavior (see Suppl. Fig. S3, e). The diffusion constants of FK-atto565

(0.21+/-0.28 $\mu m^2/s$, see also Fig. 3) and Ad2-atto565 (0.09+/-0.17 $\mu m^2/s$) were in the same range, but we noted that D for Ad2-atto565 was lower than that for FK, possibly reflecting multiple interactions of viral FK with CAR (see also Suppl. Fig. S3, d-e). We conclude that CAR mediates diffusion of virus particles on the cell surface.

Viral drifting motions upstream of internalization are mediated by CAR

Similar to diffusion, drifting motions occur upstream of internalization (Fig. 2c,d,e,f). Interestingly, most of the internalizing particles were engaged at least once in drifts (13 of 20, Fig. 2e). These viruses spent about 30% of their surface life-time in drifting motions, compared to 14% for the overall particles (4571 events), and less time in confinement (43% compared to 58%, Fig. 2d). This does not necessarily indicate that drifts promoted virus movement towards sites where endocytosis was active, but could simply reflect the fact that endocytosis-competent viruses were less likely to be trapped. Interestingly, the drifts were typically shorter than 2 µ m (Fig. 2h), and frequently interrupted by confined motions (Fig. 1a, tracks 2, 4) or diffusion (Fig. 2c). The drift speeds of internalizing Ad2-atto565 were 5-33 nm/s (Fig. 2g), which is within the range of the population drift speeds, and similar to the acto-myosin mediated drifts of murine leukemia virus (Lehmann et al., 2005), human papilloma virus (Schelhaas et al., 2008) or treadmilling rates of actin filaments (Gardel et al., 2008).

Importantly, drifting motions were observed with purified FK-atto565 at speeds between 20 and 70 nm/s, slightly higher than Ad2-atto565 particles (Fig. 3a, b). This difference is most likely due to lower image acquisition rates (0.16 Hz compared to 25 Hz for virus experiments), which was necessary to minimize the bleaching of weakly fluorescent FK (Fig. 3a, b). The drift lengths of FK ranged from 300 to 600 nm (Fig. 3c), a bit shorter than the Ad2-atto565 drifts, most likely due to bleaching of FK-atto565. Although the FK drifts amounted to only about 2% of the total lifetime, they were strongly reduced by cytoD (Fig. 3d), indicating

an actin-based mechanism similar to Ad2-atto565. Taken together, the results show that binding of the trimeric FK to CAR is sufficient for both diffusive and drifting motions.

Adenovirus targeted to αv integrins in the absence of CAR has reduced drifts and infection

We next addressed the role of αv integrin co-receptors for adenovirus motions on the surface. We used a mutant virus with a cysteine-constrained RGD motif in the FK (Ad5-RGD4C). This virus binds to αv-integrins with high affinity and attaches to CAR-negative cells (Nagel et al., 2003). Segmentation of Ad5-RGD4C-atto565 trajectories on CAR-negative L929 cells showed that the drifts were reduced to 3%, compared to 10% or 13% on CAR-expressing L929 cells for Ad5-RGD4C-atto565 or Ad2-atto565, respectively (Fig. 4a). This confirmed that Ad2 binding to CAR increases the drifts. Notably, the drifts were independent of the cytosolic tail or the transmembrane domain of CAR, as indicated by Ad2-atto565 motion analyses in L929 cells expressing glycosyl-phosphatidyl-inositol (GPI)-CAR or tailless CAR (Suppl. Fig. S4A). GPI-CAR supports infection of cultured cells similarly as full length CAR (Wang and Bergelson, 1999).

To test whether αv-integrins negatively affected drifts Ad2-atto565 was imaged on αv-integrin deficient M21L cells. The virus drifted 18% of its cell surface time. In contrast, drifts in αv-integrins expressing M21 cells, or αv-integrin overexpressing M21L4 cells were reduced to 10% or 4%, respectively (Fig. 4a), indicating that αv-integrins were not required for but reduced virus drifts. This was confirmed by the observation that integrin-bound Ad5-RGD4C-atto565 particles were confined during 90% of their cell surface time (Fig. 4a), and the remaining diffusive motions of Ad5-RGD4C-atto565 on CAR-negative L929 cells were slower than those of Ad5-RGD4C-atto565 or Ad2-atto565 on CAR-expressing L929 cells (Suppl. Fig. S4B). In addition, Ad2-atto565 motion analyses on M21 cells indicated that cRGD peptides increased the drifts from 7% to 15%, and slightly reduced confined

motions (Fig. 4b). cRGD peptides inhibit virus-integrin interactions by competing for αv -integrin binding to the viral penton-base protein (Chiu et al., 1999). Likewise, soluble extracellular αv and β3 integrin subunits fused C-terminally to human immunoglobulin Fc (αvβ3ex-Fc, see Suppl. Fig. S4C, a-b) increased viral drifts and slightly reduced the confined motions on HER-911 cells (Fig. 4b). Plasmon resonance experiments indicated that αvβ3ex-Fc binds to Ad2 (Suppl. Fig. S4C, c), and thus αvβ3ex-Fc inhibits interaction of virus with cell surface αv-integrins. αvβ3ex-Fc bound to virus less efficiently than a protein containing the extracellular domain of CAR linked to human immunoglobulin Fc (CARex-Fc, Suppl. Fig. S4C, d,e), but this is in agreement with a reported 10-fold lower affinity of αv integrins to Ad2 than soluble CAR (Chiu et al., 1999; Mayr and Freimuth, 1997; Wickham et al., 1993). We conclude that virus binding to αv integrins reduces CAR-mediated drifts.

Importantly, the specific infectivity of integrin-targeted GFP-expressing Ad5-RGD4C-atto565 in CAR-deficient human melanoma M950710 cells (M95) was about 44% lower than the infectivity in M95-CAR cells, as indicated by cold-synchronized infection (Fig. 4c-e). In addition, the treatment of L929-CAR cells with blebbistatin reduced infection with Ad5-GFP by more than 50% (Fig. 4f-g). Collectively, these data indicate that the CAR-mediated drifts promote infection.

CAR-mediated drifts and αv-integrin confinements enhance the shedding of viral fibers

We next addressed if virus drifts and confinement were involved in fiber shedding from the particles. Shedding of fibers from Ad2 on the cell surface is important for infection, and enhances virus escape from endosomes (Greber et al., 1996; Nakano et al., 2000). In vitro experiments have suggested that fiber shedding could contribute to the exposure of the membrane-active internal viral protein VI (Maier et al., 2010; Wiethoff et al., 2005; Wodrich et al., 2010). Immune-gold labeling of cryo-sections from HER-911 cells infected with Ad2 showed that cytoD

or blebbistatin prevented the reduction of fiber epitopes on Ad2 20 min post infection, compared to non-treated cells (Fig. 5a-c, e). As expected, TS1, which is deficient in fiber shedding (Greber et al., 1996), had high levels of fiber epitopes (Fig. 5d-e). Confocal laser scanning fluorescence microscopy confirmed these data, and showed that blebbistatin or cytoD treated HeLa cells were impaired at releasing fibers from incoming Ad2-atto565 (Suppl. Fig. S5, a-b).

A rabbit polyclonal anti-fiber antibody was used in experiments described in Fig. 5 and Suppl. Fig. S5, but the results were confirmed also with a monoclonal anti-fiber antibody 6A4 (data not shown, Fender et al., 1995). Unfortunately, fiber-shedding could not be compared in M95 and M95-CAR cells, since infection of CAR-negative cells requires Ad5-RGD4C virus and anti-fiber antibodies (and 6A4) are specific for Ad2 (not shown).

Biochemical assays had previously shown that fiber shedding and virus infection are inhibited by cRGD peptides in HeLa cells (Greber et al., 1996; Nakano et al., 2000; Wickham et al., 1994; Wickham et al., 1993). When analyzed by confocal laser scanning fluorescence microscopy, fiber shedding from Ad2-atto565 in αv-integrin-negative M21L cells was less efficient than in αv-integrin overexpressing M21L4 cells (Suppl. Fig. S5, c-d). In contrast to cRGD peptides, soluble αvβ3ex-Fc did not affect fiber shedding from incoming Ad2 in HER-911 cells (Fig. 6a-b), although αvβ3ex -Fc inhibited Ad5-GFP infection of HER-911 cells and M21L4 cells (Fig. 6c-d), and the release of incoming virus to the cytosol (not shown). This is consistent with earlier observations showing that integrins are important for adenovirus internalization and membrane penetration (Greber et al., 1996; Wickham et al., 1994; Wickham et al., 1993). Taken together, these results suggest that both the CAR-mediated drifts and interaction of virus with integrins are required for efficient fiber-shedding. Soluble integrins can substitute for membrane-anchored integrins in fiber shedding, but not in viral escape to the cytosol.

CAR-mediated drifts enhance the exposure of the membrane-lytic internal capsid protein VI

The escape of adenovirus from endosomes to the cytosol is coupled to partial uncoating of the capsid at the plasma membrane and in endosome, as indicated by entry analyses of the uncoating defective mutant TS1 (Gastaldelli et al., 2008). These early uncoating events involve the release of fibers, penton base and internal capsid proteins, such as proteins IIIa and VIII (Greber et al., 1993; Nakano et al., 2000). The membrane lytic factor of adenovirus is protein VI located within the capsid (Perez-Berna et al., 2009; Silvestry et al., 2009; Wiethoff et al., 2005). Protein VI epitopes were found to be exposed during virus entry (Wodrich et al., 2010). We raised a polyclonal antiserum against protein VI, which allows quantitative *in situ* analyses of protein VI during entry. This antibody did not react with native Ad2, unlike the R72 fiber-specific antibody (Suppl. Fig. S6A, a-c). Likewise, purified Ad5-RGD4C was negative for anti-protein VI staining, as well as viruses used for cryo-EM experiments (Suppl. Fig. S6A, d). Ultrathin cryo-EM sections of infected cells were used to assess total protein VI in incoming virions. As expected, both Ad2 and TS1 particles on the cell surface or endosomes were positive for protein VI, but cytosolic Ad2 lacked protein VI (Fig. 7a,b). This indicated that protein VI was lost from incoming Ad2 virions before or during endosomal penetration.

We next analyzed if protein VI was exposed on incoming virus particles. Using confocal laser scanning microscopy we found that the exposure of protein VI was maximal at 10 min post warming in cold synchronized HeLa infections (Fig. 7c, and Suppl. Fig. S6B). Essentially no exposed protein VI epitopes were detectable in cell surface virions (Fig. 7c), and TS1 showed no change in protein VI epitopes from 0 to 10 min post infection (not shown). Time course experiments suggested that protein VI was exposed at or shortly after virus uptake into endosomes (data not shown).

Interestingly, we also detected protein VI epitopes devoid of atto565 labeling, suggesting that protein VI separated from the viral capsids (Fig. 7c, 10 min). The inhibition of acto-myosin by blebbistatin or cytoD strongly reduced the exposure of protein VI epitopes at 10 min pi, and inhibition of virus-integrin interactions by cRGD peptides also inhibited protein VI exposure, albeit less efficiently (Fig. 7d). This latter result was confirmed in αv-integrin lacking M21L cells, which were found to promote protein VI epitope exposure less efficiently than the αv-integrin overexpressing M21L4 cells (Fig. 7e, and Suppl. Fig. S6C). Taken together, these results suggest that acto-myosin mediated drifts together with virus-integrin interactions support efficient protein VI exposure.

Importantly, the Ad5-RGD4C particles targeted to integrins in CAR-deficient L929 cells had a significantly lower level of exposed protein VI epitopes than the L929 CAR-positive cells at 10 min post warming (Fig. 7f, and Suppl. Fig. S6D). This was not due to different rates of viral endocytosis, since when uptake of Ad5-RGD4C-atto565 was measured by anti-hexon surface stain 68.2% of particles in L929 and 66.4% in L929-CAR cells were found to be endocytozed at the 10 min time point (not shown). These results specifically show that the ability of CAR to drift enhanced protein VI exposure.

Discussion

Based on our data and previous research we propose the following model. Immediately after binding to the surface, adenovirus diffuses on CAR for many seconds (Suppl. Fig. S7, step 1). This motion is similar to the diffusion of virus-free CAR, and allows rapid scanning over large areas of plasma membrane. The diffusive motions become less frequent with prolonged surface residence during

the first minutes of infection, before virus internalization. Decreased diffusion coincides with increasing drifting and confined motions, and suggests that virus progressively interacts with multiple receptors (Suppl. Fig. S7, step 2). Clustering of CAR may trigger CAR drifts that are driven by dynamic actin filament turnover and the action of myo2. Drifting CAR receptors together with immobile integrins induce fiber shedding (Suppl. Fig. S7, step 3). We can envision two non-exclusive mechanisms for fiber shedding. In the first mechanism, CAR is pulling on virus, which leads to drifts, and fiber-capsid connections break, leaving fiber behind, while virus continues to drift on CAR bound to fibers that are still attached to the virus. In the second mechanism, CAR is pulling on fiber and breaks the connection by moving away thereby leaving the capsid behind. Our experiments tracked the viruses and determined the drifting motions of viruses and FK in the first mechanism, while our imaging was not sensitive enough to directly observe the second mechanism. We hypothesize that integrin binding to penton base induces a conformational change that further weakens the interaction between the capsid and the penton-fiber complex (Lindert et al., 2009). In the presence of a pulling force exerted by CAR linked to the acto-myosin machinery this may release fibers from penton-base. Subsequently protein VI is exposed from the capsid (Suppl. Fig. S7, step 4). Possibly, this situation involves mechanical strain on the capsid vertex through opposing CAR-mediated drifts and integrin-mediated confinement actions. Fiber release and protein VI exposure are key for activating the endosome escape machinery of the virus (Greber et al., 1996; Maier et al., 2010; Moyer et al., 2011; Wiethoff et al., 2005).

A key finding of this work is that drifting motions occur by FK interactions with CAR, and can be observed with recombinant trimeric FK and virus particles. The trimeric FK can cluster CAR, but the ability of virus-free/FK free CAR to drift was not tested. This suggests that CAR-drifts are virus-induced, and occur by clustering of CAR. The trimeric FK is known to bind to three D1 domains of CAR, as shown by kinetic measurements (Lortat-Jacob et al., 2001), and FRAP analyses. CAR clustering by FK is further supported by a crystal structure of D1,

where D1 forms a dimer (van Raaij et al., 2000), and by cryo-EM structures of full length CAR in a complex with coxsackievirus, where the C-termini of two CAR molecules stick together (He et al., 2001). Thus, CAR clustering by FK may engage an avidity mechanism and enhance infection (Lortat-Jacob et al., 2001), as well as drifting motions.

Interestingly, drifting motions are observed with GPI-linked CAR lacking transmembrane and cytosolic domains (Suppl. Fig. S4A), and GPI-CAR fully supports infection (see also, Wang and Bergelson, 1999). The drifts of GPI-linked CAR could involve glyco-sphingolipids and cholesterol-rich membrane domains (Varma and Mayor, 1998) that would enhance CAR clustering. In fact, the binding of mouse polyomavirus to ganglioside-glycolipids triggers drifts, apparently in the absence of direct contacts of the virus with a transmembrane protein (Ewers et al., 2005).

The adenovirus-triggered CAR-drifts depend on dynamic actin filaments and myosin-2, as shown by chemical interference. This is similar to other receptors mediating retrograde motions of viruses on filopodia, such as retroviruses, polyomavirus, papillomavirus or vaccinia virus (reviewed in Burckhardt and Greber, 2009). Our finding that the adenovirus engages with drifting CAR on the cell body and thereby enhances infection, suggests an additional function for CAR than just attaching the virus to the plasma membrane. This function is not related to searching for a particular site on the plasma membrane, since viral motions by diffusion were not sufficient to give rise to full infection. Instead, the binding of adenovirus to CAR triggers drifting motions, and together with integrins, this provides a cue for fiber shedding and the exposure of the membrane-active internal protein VI. Both steps are inhibited in blebbistatin or cytoD treated cells, and protein VI exposure is reduced in CAR-negative L929 cells compared to L929-CAR positive cells. CAR-mediated drifts are unlikely to promote virus infection merely by enhancing virus binding to integrins, since Ad5-RGD4C, which is capable of directly binding to integrins without CAR, is less

infectious and exposes protein VI less efficiently than the same virus on CAR-positive cells.

Integrins are not involved in adenovirus drifts but associated with virus confinement. Interference with virus-integrin interactions increases the drifts and reduces the confined motions, as well as fiber shedding and protein VI exposure. These results suggest that fiber-shedding and protein VI exposure are dependent on both the CAR-drifts and virus-integrin interactions. These events may occur simultaneously. Interestingly, the binding of soluble αvβ5 to the RGD loop of the Ad12 penton-base untwists the penton-base pentamer (Lindert et al., 2009), possibly weakening the stability of the capsid vertex. In fact, our results demonstrate that soluble integrins allow fiber shedding but inhibit infection, whereas cRGD peptides, which compete for integrin binding to penton-base block fiber shedding (Nakano et al., 2000; Wickham et al., 1993).

In conclusion, this report shows that drifting motions and coreceptor confinement activate a viral membrane lytic factor. Other viruses may use similar strategies for their uncoating programs.

Experimental Procedures

Live cell microscopy

Adenovirus motions were recorded by spinning disc confocal microscopy at 37°C for 90-600 seconds at a frequency of 2-25 Hz between 0 to 10 min after virus addition to cells, as described (Helmuth et al., 2007). Images were recorded on a Cascade 512 EM-CCD camera (Photometrics) with an N.A. 1.35 UplanApo100x objective on an Olympus IX81 inverted microscope (Olympus Switzerland) equipped with a temperature controlled incubator box (Life imaging services,

Basel, Switzerland), a Yokogawa scanning head QLC100 (VisiTech International) with triple band-pass excitation (488 nm/565 nm/647 nm) and emission filters (Chroma), and an Innova 70C mixed-gas laser (Coherent). Total internal reflection fluorescence (TIRF) microscopy was performed as described (Helmuth et al., 2007). For multichannel recordings, images were acquired sequentially.

Single particle tracking and trajectory segmentations

Single particle tracking (Sbalzarini and Koumoutsakos, 2005) and trajectory segmentation (Helmuth et al., 2007) were performed from data acquired by live imaging experiments as described. Confidence intervals for the median of the fractions of motion types were estimated by bootstrapping (Helmuth et al., 2007). Diffusion constants, drift speeds and lengths were calculated from the segmented tracks. The precision of borders between the different motion types were estimated with *in silico* trajectories and gave 90-99.8% correct identifications of the individual motion steps (Helmuth et al., 2007). This precision was sufficient considering the very high heterogeneity of viral tracks. Diffusion was identified as a motion pattern, which looked significantly different from the drifts and the confined motions. It is not to be confused with pure random walks, which can be seen at the plasma membrane with super high speed imaging (Kusumi et al., 2005) (see MSS slope analysis in Supplemental Fig. S2). All image and data analysis was done with Matlab (The Mathworks).

Dynamin2-EGFP and virus co-internalization

Images were recorded on the Olympus IX81 in TIRF mode at 1 Hz in the Ad2-atto565 channel and 0.5 Hz in the EGFP channel during the first 10 min of infection. The virus images were subjected to particle tracking and trajectory segmentation. Image sequences were analyzed manually and internalization events selected where a virus particle disappeared from the TIRF view simultaneously with a short peak in dynamin2-EGFP intensity. Selected

trajectories were subjected to trajectory segmentation, and tracks aligned at their start.

Immunofluorescence assay for fiber release and protein VI exposure

Cells were treated with drugs, infected, stained with the R72 anti-fiber antibody (Baum et al., 1972), and processed for confocal microscopy as described in Supplemental Experimental Procedures. MacBiophotonics ImageJ (http://www.macbiophotonics.ca/downloads.htm) was used for image processing of Fig. 7c. The level of antibody staining was determined on the position of the viruses. Mean antibody intensities were calculated for each cell and plotted as boxplots where the middle horizontal line represents the median, the lower end of the box is the 25th percentile and the upper end of the box is the 75th percentile of the distribution. Bars span the entire distribution excluding the outliers that are plotted as plus signs. The medians of two distributions were compared using the Wilcoxon rank sum test. Analysis of protein VI exposure in infected HeLa, M21L vs M21L4 or L929 vs L929-CAR cells was done as described for fiber release.

Virus endocytosis

Cells, viruses and antibodies were used as described in Supplemental Experimental Procedures. Analyses occurred by a Matlab-based routine (Puntener et al., 2011).

Cryo-section EM

Cryo-sections were prepared according to the Tokuyasu method (Slot and Geuze, 2007).

For additional information see supplemental information.

Acknowledgements

We thank Curzio Rüegg (University of Lausanne) for integrin-Fc constructs, Bernhard Wehrle-Haller (University Hospital of Geneva) for the actin-EGFP construct, Mark McNiven (Mayo Clinic, Rochester, USA) for Dyn2-EGFP, Jeff Bergelson (The Children's Hospital of Philadelphia, USA) for CAR, CAR-GPI and CAR-tailless constructs. We thank Urs Ziegler (Center for Microscopy and Image Analysis, University of Zurich) for instructions concerning FRAP measurements, Stefan Schauer (Functional Genomics Center, University of Zurich), Trinh Hung Viet, Andreas Jurgeit and Leta Fuchs (Institute of Molecular Life Sciences, University of Zurich) for Biacore support, high throughput image-based data acquisition or purifying soluble integrins, and Ari Helenius and Helge Ewers (ETH Zurich) for access and introduction to TIRF microscopy. The work was supported by grants from the Swiss National Science Foundation, the Swiss SystemsX.ch initiative, grant LipidX-2008/011 and the Novartis Research foundation to UFG.

Author contributions

CJB and UFG initiated the study, and UFG coordinated the study. CJB, MS, PS, SH, UFG designed experiments. CJB performed most experiments, except Fig. 1b (PS), 6 (UFG and KB), 5a-e (KB), Fig. 7 (MS), Suppl. Fig. S6 (MS), CJB, PS, KB, SH, MS, UFG analyzed experiments. SH provided essential reagents. CJB, MS and UFG wrote the manuscript.

Competing financial interests

The authors declare no competing financial interests.

References

Baum, S.G., Horwitz, M.S., and J.V. Maizel, J. (1972). Studies of the mechanism of enhancement of human adenovirus infection in monkey cells by simian virus 40. J Virol *10*, 211-219.

Bergelson, J.M., Cunningham, J.A., Droguett, G., Kurt-Jones, E.A., Krithivas, A., Hong, J.S., Horwitz, M.S., Crowell, R.L., and Finberg, R.W. (1997). Isolation of a common receptor for Coxsackie B viruses and adenoviruses 2 and 5. Science *275*, 1320-1323.

Bewley, M.C., Springer, K., Zhang, Y.B., Freimuth, P., and Flanagan, J.M. (1999). Structural analysis of the mechanism of adenovirus binding to its human cellular receptor, CAR. Science *286*, 1579-1583.

Burckhardt, C.J., and Greber, U.F. (2009). Virus movements on the plasma membrane support infection and transmission between cells. PLoS Pathog *5*, e1000621.

Chiu, C.Y., Mathias, P., Nemerow, G.R., and Stewart, P.L. (1999). Structure of adenovirus complexed with its internalization receptor, alpha(v)beta 5 integrin. J Virol *73*, 6759-6768.

Coyne, C.B., and Bergelson, J.M. (2005). CAR: a virus receptor within the tight junction. Adv Drug Deliv Rev *57*, 869-882.

Cureton, D.K., Massol, R.H., Saffarian, S., Kirchhausen, T.L., and Whelan, S.P. (2009). Vesicular stomatitis virus enters cells through vesicles incompletely coated with clathrin that depend upon actin for internalization. PLoS Pathog *5*, e1000394.

Danowski, B.A. (1989). Fibroblast contractility and actin organization are stimulated by microtubule inhibitors. Journal of cell science *93 (Pt 2)*, 255-266.

Doherty, G.J., and McMahon, H.T. (2009). Mechanisms of endocytosis. Annu Rev Biochem *78*, 857-902.

Ebert, D.H., Deussing, J., Peters, C., and Dermody, T.S. (2002). Cathepsin L and cathepsin B mediate reovirus disassembly in murine fibroblast cells. J Biol Chem *277*, 24609-24617.

Ewers, H., Smith, A.E., Sbalzarini, I.F., Lilie, H., Koumoutsakos, P., and Helenius, A. (2005). Single-particle tracking of murine polyoma virus-like particles on live cells and artificial membranes. Proc Natl Acad Sci U S A *102*, 15110-15115.

Fender, P., Kidd, A.H., Brebant, R., Oberg, M., Drouet, E., and Chroboczek, J. (1995). Antigenic sites on the receptor-binding domain of human adenovirus type 2 fiber. Virology *214*, 110-117.

Gardel, M.L., Sabass, B., Ji, L., Danuser, G., Schwarz, U.S., and Waterman, C.M. (2008). Traction stress in focal adhesions correlates biphasically with actin retrograde flow speed. J Cell Biol *183*, 999-1005.

Gastaldelli, M., Imelli, N., Boucke, K., Amstutz, B., Meier, O., and Greber, U.F. (2008). Infectious adenovirus type 2 transport through early but not late endosomes. Traffic *9*, 2265-2278.

Greber, U.F., Webster, P., Weber, J., and Helenius, A. (1996). The role of the adenovirus protease on virus entry into cells. Embo J *15*, 1766-1777.

Greber, U.F., Willetts, M., Webster, P., and Helenius, A. (1993). Stepwise dismantling of adenovirus 2 during entry into cells. Cell *75*, 477-486.

Hayashi, S., and Hogg, J.C. (2007). Adenovirus infections and lung disease. Curr Opin Pharmacol *7*, 237-243.

He, Y., Chipman, P.R., Howitt, J., Bator, C.M., Whitt, M.A., Baker, T.S., Kuhn, R.J., Anderson, C.W., Freimuth, P., and Rossmann, M.G. (2001). Interaction of coxsackievirus B3 with the full length coxsackievirus-adenovirus receptor. Nat Struct Biol *8*, 874-878.

Helmuth, J.A., Burckhardt, C.J., Koumoutsakos, P., Greber, U.F., and Sbalzarini, I.F. (2007). A novel supervised trajectory segmentation algorithm identifies distinct types of human adenovirus motion in host cells. J Struct Biol *159*, 347-358.

Hierholzer, J. (1992). Adenoviruses in the immunocompromised host. Clin Microbiol Rev *5*, 262-274.

Imelli, N., Ruzsics, Z., Puntener, D., Gastaldelli, M., and Greber, U.F. (2009). Genetic reconstitution of the human adenovirus type 2 temperature-sensitive 1 mutant defective in endosomal escape. Virol J *6*, 174.

Krendel, M., Zenke, F.T., and Bokoch, G.M. (2002). Nucleotide exchange factor GEF-H1 mediates cross-talk between microtubules and the actin cytoskeleton. Nature cell biology *4*, 294-301.

Kusumi, A., Nakada, C., Ritchie, K., Murase, K., Suzuki, K., Murakoshi, H., Kasai, R.S., Kondo, J., and Fujiwara, T. (2005). Paradigm shift of the plasma membrane concept from the two-dimensional continuum fluid to the partitioned fluid: high-speed single-molecule tracking of membrane molecules. Annu Rev Biophys Biomol Struct *34*, 351-378.

Lehmann, M.J., Sherer, N.M., Marks, C.B., Pypaert, M., and Mothes, W. (2005). Actin- and myosin-driven movement of viruses along filopodia precedes their entry into cells. J Cell Biol *170*, 317-325.

Li, E., Stupack, D., Bokoch, G.M., and Nemerow, G.R. (1998). Adenovirus endocytosis requires actin cytoskeleton reorganization mediated by Rho family GTPases. J Virol *72*, 8806-8812.

Lindert, S., Silvestry, M., Mullen, T.M., Nemerow, G.R., and Stewart, P.L. (2009). Cryo-electron microscopy structure of an adenovirus-integrin complex indicates conformational changes in both penton base and integrin. J Virol *83*, 11491-11501.

Liu, H., Jin, L., Koh, S.B., Atanasov, I., Schein, S., Wu, L., and Zhou, Z.H. (2010). Atomic structure of human adenovirus by cryo-EM reveals interactions among protein networks. Science *329*, 1038-1043.

Lortat-Jacob, H., Chouin, E., Cusack, S., and van Raaij, M.J. (2001). Kinetic analysis of adenovirus fiber binding to its receptor reveals an avidity mechanism for trimeric receptor-ligand interactions. J Biol Chem *276*, 9009-9015.

Lutschg, V., Boucke, K., Hemmi, S., and Greber, U. (2011). Chemotactic anti-viral cytokines promote infectious apical entry of human adenovirus into polarized epithelial cells. In Nat Commun (Nature Publishing Group), pp. DOI: 10.1038/ncomms1391.

Maier, O., Galan, D.L., Wodrich, H., and Wiethoff, C.M. (2010). An N-terminal domain of adenovirus protein VI fragments membranes by inducing positive membrane curvature. Virology *402* 11-19.

Mayr, G.A., and Freimuth, P. (1997). A single locus on human chromosome 21 directs the expression of a receptor for adenovirus type 2 in mouse A9 cells. J Virol *71*, 412-418.

Meier, O., Boucke, K., Hammer, S.V., Keller, S., Stidwill, R.P., Hemmi, S., and Greber, U.F. (2002). Adenovirus triggers macropinocytosis and endosomal leakage together with its clathrin-mediated uptake. J Cell Biol *158*, 1119-1131.

Mercer, J., Schelhaas, M., and Helenius, A. (2010). Virus Entry by Endocytosis. Annu Rev Biochem *79*, 803-833.

Merrifield, C.J., Feldman, M.E., Wan, L., and Almers, W. (2002). Imaging actin and dynamin recruitment during invagination of single clathrin-coated pits. Nat Cell Biol *4*, 691-698.

Mothes, W., Sherer, N.M., Jin, J., and Zhong, P. (2010). Virus cell-to-cell transmission. J Virol *84*, 8360-8368.

Moyer, C.L., Wiethoff, C.M., Maier, O., Smith, J.G., and Nemerow, G.R. (2011). Functional genetic and biophysical analyses of membrane disruption by human adenovirus. J Virol *85*, 2631-2641.

Nagel, H., Maag, S., Tassis, A., Nestle, F.O., Greber, U.F., and Hemmi, S. (2003). The alphavbeta5 integrin of hematopoietic and nonhematopoietic cells is a transduction receptor of RGD-4C fiber-modified adenoviruses. Gene Ther *10*, 1643-1653.

Nakano, M.Y., Boucke, K., Suomalainen, M., Stidwill, R.P., and Greber, U.F. (2000). The first step of adenovirus type 2 disassembly occurs at the cell surface, independently of endocytosis and escape to the cytosol. J Virol *74*, 7085-7095.

Odegard, A.L., Kwan, M.H., Walukiewicz, H.E., Banerjee, M., Schneemann, A., and Johnson, J.E. (2009). Low endocytic pH and capsid protein autocleavage are critical components of Flock House virus cell entry. J Virol *83*, 8628-8637.

Perez-Berna, A.J., Marabini, R., Scheres, S.H., Menendez-Conejero, R., Dmitriev, I.P., Curiel, D.T., Mangel, W.F., Flint, S.J., and San Martin, C. (2009). Structure and uncoating of immature adenovirus. J Mol Biol *392*, 547-557.

Perrais, D., and Merrifield, C.J. (2005). Dynamics of endocytic vesicle creation. Dev Cell *9*, 581-592.

Puntener, D., Engelke, M.F., Ruzsics, Z., Strunze, S., Wilhelm, C., and Greber, U.F. (2011). Stepwise loss of fluorescent core protein V from human adenovirus during entry into cells. J Virol *85*, 481-496.

Reddy, V.S., Natchiar, S.K., Stewart, P.L., and Nemerow, G.R. (2010). Crystal structure of human adenovirus at 3.5 A resolution. Science *329*, 1071-1075.

Roelvink, P.W., Mi Lee, G., Einfeld, D.A., Kovesdi, I., and Wickham, T.J. (1999). Identification of a conserved receptor-binding site on the fiber proteins of CAR-recognizing adenoviridae. Science *286*, 1568-1571.

Sbalzarini, I.F., and Koumoutsakos, P. (2005). Feature point tracking and trajectory analysis for video imaging in cell biology. J Struct Biol *151*, 182-195.

Schelhaas, M., Ewers, H., Rajamaki, M.L., Day, P.M., Schiller, J.T., and Helenius, A. (2008). Human papillomavirus type 16 entry: retrograde cell surface transport along actin-rich protrusions. PLoS Pathogens *4*, e1000148.

Schelhaas, M., Malmstrom, J., Pelkmans, L., Haugstetter, J., Ellgaard, L., Grunewald, K., and Helenius, A. (2007). Simian Virus 40 depends on ER protein folding and quality control factors for entry into host cells. Cell *131*, 516-529.

Sherer, N.M., Lehmann, M.J., Jimenez-Soto, L.F., Horensavitz, C., Pypaert, M., and Mothes, W. (2007). Retroviruses can establish filopodial bridges for efficient cell-to-cell transmission. Nat Cell Biol *9*, 310-315.

Silvestry, M., Lindert, S., Smith, J.G., Maier, O., Wiethoff, C.M., Nemerow, G.R., and Stewart, P.L. (2009). Cryo-electron microscopy structure of adenovirus type 2 temperature-sensitive mutant 1 reveals insight into the cell entry defect. J Virol *83*, 7375-7383.

Slot, J.W., and Geuze, H.J. (2007). Cryosectioning and immunolabeling. Nat Protoc *2*, 2480-2491.

Smyth, M.S., and Martin, J.H. (2002). Picornavirus uncoating. Mol Pathol *55*, 214-219.

Soulet, F., Yarar, D., Leonard, M., and Schmid, S.L. (2005). SNX9 regulates dynamin assembly and is required for efficient clathrin-mediated endocytosis. Mol Biol Cell *16*, 2058-2067.

Stewart, P.L., and Nemerow, G.R. (2007). Cell integrins: commonly used receptors for diverse viral pathogens. Trends Microbiol *15*, 500-507.

Straight, A.F., Cheung, A., Limouze, J., Chen, I., Westwood, N.J., Sellers, J.R., and Mitchison, T.J. (2003). Dissecting temporal and spatial control of cytokinesis with a myosin II Inhibitor. Science *299*, 1743-1747.

Tsang, S.K., McDermott, B.M., Racaniello, V.R., and Hogle, J.M. (2001). Kinetic analysis of the effect of poliovirus receptor on viral uncoating: the receptor as a catalyst. J Virol *75*, 4984-4989.

van Raaij, M.J., Chouin, E., van der Zandt, H., Bergelson, J.M., and Cusack, S. (2000). Dimeric structure of the coxsackievirus and adenovirus receptor D1 domain at 1.7 A resolution. Structure Fold Des *8*, 1147-1155.

Varma, R., and Mayor, S. (1998). GPI-anchored proteins are organized in submicron domains at the cell surface. Nature *394*, 798-801.

Wang, K., Huang, S., Kapoor-Munshi, A., and Nemerow, G. (1998). Adenovirus internalization and infection require dynamin. J Virol *72*, 3455-3458.

Wang, X.H., and Bergelson, J.M. (1999). Coxsackievirus and adenovirus receptor cytoplasmic and transmembrane domains are not essential for coxsackievirus and adenovirus infection. Journal of Virology *73*, 2559-2562.

Wickham, T.J., Filardo, E.J., Cheresh, D.A., and Nemerow, G.R. (1994). Integrin $\alpha v\beta 5$ selectively promotes adenovirus mediated cell membrane permeabilization. J Cell Biol *127*, 257-264.

Wickham, T.J., Mathias, P., Cheresh, D.A., and Nemerow, G.R. (1993). Integrins alpha v beta 3 and alpha v beta 5 promote adenovirus internalization but not virus attachment. Cell *73*, 309-319.

Wiethoff, C.M., Wodrich, H., Gerace, L., and Nemerow, G.R. (2005). Adenovirus protein VI mediates membrane disruption following capsid disassembly. J Virol *79*, 1992-2000.

Witherden, D.A., Verdino, P., Rieder, S.E., Garijo, O., Mills, R.E., Teyton, L., Fischer, W.H., Wilson, I.A., and Havran, W.L. (2010). The junctional adhesion molecule JAML is a costimulatory receptor for epithelial gammadelta T cell activation. Science *329*, 1205-1210.

Wodrich, H., Henaff, D., Jammart, B., Segura-Morales, C., Seelmeir, S., Coux, O., Ruzsics, Z., Wiethoff, C.M., and Kremer, E.J. (2010). A capsid-encoded PPxY-motif facilitates adenovirus entry. PLoS Pathog *6*, e1000808.

Figure legends

Fig. 1: Ad2 drifts depend on actin retrograde flow and myosin-2 and support infection.

(**a**) Automated segmentation of 25 Hz trajectories of Ad2-atto565 shows drifts (red), diffusion (cyan), confined motion (black) and not classified motion (dark blue). Example trajectories of viruses bound to filopodia (trajectories1-3) or the cell body (trajectories 4+5) are depicted.

(**b**) Quantification of Ad2-atto565 motion patterns on filopodia and the cell body of HER-911 cells during the first 5 min post inoculation. Cells were either untreated (no drug) or pretreated for 20 min with 50 µM blebbistatin (Blebbi) or 5 µM cytoD. The drugs were present during imaging. The median time of viruses in each motion type is plotted, including 95% confidence intervals (bootstrapping). c = number of cells, t = number of analyzed trajectories.

See also Suppl. Fig. S1 and Mov. S1-2.

Fig. 2: Drifts, diffusion and confined motions occur on Ad2 prior to internalization.

(**a-c**) Ad2-atto565 was added to HER-911 cells stably expressing dynamin2-EGFP and imaged immediately thereafter for 10 min. Images were recorded at 1Hz in the red channel (568nm) and 0.5 Hz in the green channel (488nm). Virus internalization events were identified by visual inspection, when Ad2-atto565 particles disappeared from the TIRF view simultaneously with a blink of dynamin2-EGFP. One such event is shown in (a), where a virus (red) binds at t = 0 and is internalized 421 s after binding, with a dynamin2-EGFP (green) peak at 406 s. The corresponding image intensity profiles for Ad2-atto565 and dynamin2-EGFP are shown in (b), and the segmented trajectory of the virus in (c), including start and end positions. The part of the trajectory that occurred during the

dynamin2-EGFP peak shown is plotted as thick red line close to the end of the track (399-420 s after virus binding).

(**d**) The quantification of motion patterns of Ad2-atto565 on HER-911 expressing dynamin2-EGFP, including the internalizing viruses (t=20) and the entire population of analyzed viruses (t=4571). The median time of viruses in each motion type is plotted (95% confidence intervals from bootstrapping). c = number of cells recorded, t = number of analyzed trajectories. Color code as in (c).

(**e**) Profiles of motion patterns from the trajectories of internalizing Ad2-atto565 aligned to the time of virus binding to the cells at t = 0. Color code as in (c).

(**f**) Analysis of the frequency of motion types calculated for every frame in the aligned tracks in panel (e) for the first 200 s after virus binding to the cell. Color code as in (c).

(**g-h**) Drift speed and length histograms for internalizing Ad2-atto565 (depicted in red) in the context of the entire population of viruses (black). N = number of drifts.

See also Suppl. Fig. S2 and Suppl. Mov. S3.

Fig. 3: Recombinant fiber knobs have similar drift speeds and lengths as virus particles.

Fluorescent Ad5 fiber-knobs labeled with atto565 were imaged on the surface of HER-911 cells by TIRF microscopy at 0.2 Hz. Example trajectories of drifting FK are shown in (**a**). Histograms of drift speeds and lengths from 25 tracks on 57 cells are shown in (**b**) and (**c**), respectively. (**d**) In HER-911 cells treated with cytoD (5 µM) Ad5 fiber-knob-atto565 had a significantly reduced drift median time (bootstrapping, 95% confidence intervals). c = number of cells.

See also Suppl. Fig. S3.

Fig. 4: Ad2 drifts depend on CAR but not αv-integrins, and drifts enhance infection.

(**a**) Motion analyses of Ad2-atto565 (wild type, wt) and Ad5-RGD4C-atto565 (RGD4C) on L929 (CAR-negative), L929-CAR (stably expressing human CAR), M21L (αv-integrin-negative), M21 (αv-integrin-positive) or M21L4 (αv-integrin overexpressing) cells indicating the median time of viruses in each motion type (drifts, diffusion, confinement, not classified). Data are represented as the median time the viruses spent in each motion type. 95% confidence intervals were obtained by bootstrapping. Number of cells (C) and trajectories (t) analyzed.

(**b**) M21 and Her-911 cells were pretreated for 20 min with cyclic RGD (cRGD, 0.5 mM) or soluble αvβ3ex-Fc (0.097mg/ml), respectively, and Ad2-atto656 motion patterns were analyzed after 5 min of inoculation in the presence of inhibitors. Virus trajectories were obtained and analyzed as described before, and data represented as the median time the viruses spent in each motion type. The 95% confidence intervals were obtained by bootstrapping. c = number of cells recorded, t = number of analyzed trajectories.

(**c**-**e**) Infection of CAR-expressing M950710 melanoma cells (M95-CAR) or CAR-minus M950710 cells (M95) with Ad5-RGD4C-atto565-GFP (RGD4C) targeted to αv-integrins. Input of fluorescent viruses was chosen such that equal numbers of RGD4C particles attached to M95 and M95-CAR cells 15 min post inoculation. Both cell lines are positive for αv-integrins (not shown). (**c-d**) Subsequently, cells were washed, and infection carried out for 12 h, followed by analyses of median GFP expression by fluorescence microscopy (**e**). Bootstrapping was used to obtain 95% confidence intervals.

(**f**-**g**) Mouse L929-CAR cells stably expressing human CAR were treated with blebbistatin or carrier DMSO, infected with Ad5-EGFP, fixed and DAPI stained 12 h post infection, followed by GFP intensity measurements in the DAPI area. Example images with overlaid GFP and DAPI channels are shown in panel (f), and median GFP intensities in (g), including the 95% confidence intervals (bootstrapping).

See also Suppl. Fig. S4.

Fig. 5: Ad2 drifts are required for Ad2 fiber shedding.

HER-911 cells were incubated with Ad2 in the cold and warmed for 20 min and prepared for cryo-section EM analyses. Fiber epitopes were detected with the rabbit R72 antibody and 10 nm gold coupled secondary goat anti-rabbit antibodies. Representative images are shown in (**a-d**). Gold particles are highlighted with arrowheads. (**e**) Quantification of gold particles per virus particles at the plasma membrane indicated by the mean and +/- standard error of the mean. P-values were obtained by Student's t-tests. c = number of cells, v = number of viruses analyzed.

See also Suppl. Fig. S5.

Fig. 6: Soluble integrins inhibit infection but not fiber shedding.

(**a-b**) Immune-gold labeling of cryo-EM sections for Ad2 fiber. HER-911 cells were treated with αvβ3ex-Fc or control CD46ex-Fc protein as described in Fig. 4b, followed by inoculation with Ad2-wt in cold medium and internalization at 37°C for 20 min. Cells were fixed, embedded for cryo-EM and imaged as described in the legend for Fig. 5. Plasma membrane bound viruses and gold particles depicting fiber epitopes were counted manually (b). Shown is the mean number of gold particles per virus +/- SEM (d). P-values were obtained by Student's t-test. c = number of cells, v = number of viruses analyzed. Note that there was slight experimental variability in the efficiency of fiber staining indicated by the observation of 0.17 gold particles per Ad2 in control cells in Fig. 5e, and 0.28 gold per Ad2 in Fig. 6b. This did not change, however, the conclusion that neither soluble integrins nor CD46 affected the shedding of fiber.

(**c-d**) M21L4 or HER-911 cells were treated with αvβ3ex-Fc (0.097 mg/ml, 0.015 mg/ml, 0.006 mg/ml) or control CD46ex-Fc protein (0.097 mg/ml) and infected with Ad5-GFP for 12 h. Cells were fixed, DAPI stained and imaged. Example images with overlaid DAPI and GFP signals are shown, including quantification of the median GFP intensities over the DAPI-positive area (d). The 95% confidence intervals were obtained by bootstrapping.

Fig. 7: The transient exposure of protein VI on incoming Ad2 requires drifts and integrins

(**a**) Cryo sections of Ad2 or TS1 infected HeLa cells prepared at 30 min post infection were immune-labeled with an affinity-purified anti-protein VI antibody and goat anti-rabbit coupled to 10 nm colloidal gold. Note the presence of protein VI (filled arrowheads) on cell surface attached Ad2 or endosomal TS1. Open arrowheads depict virus particles.

(**b**) Quantification of protein VI specific immune-gold on Ad2 or TS1 particles including the number of cells and virus particles analyzed. P-values are derived from two-sided t-tests.

(**c**) Immunofluorescence labeling of protein VI (green) in HeLa cells infected with Ad2-atto565 (red) for 0 or 10 min. The protein VI-positive particles are shown in yellow, some of which are pointed out by yellow arrows. Red double arrowheads indicate particles devoid of protein VI signal, and green arrowheads protein VI signal not colocalizing with virus. Cell borders are indicated by grey lines.

(**d-f**) Quantifications of protein VI immune-reactivity on Ad2-atto565 in (d) HeLa cells treated with acto-myosin inhibitors blebbistatin (50 µM) or cytochalasin D (5 µM), or with cRGD peptides (0.2 mM). (e) Virus-associated protein VI signal in M21L or M21L4 cells infected with Ad2-atto565, or (f) in L929 or L929-CAR cells inoculated with Ad5-RGD4C-atto565. In (d-e) virus was bound to cells at 0°C and internalized for the indicated times, whereas in (e) virus was bound and internalized into cells at 37°C for 20 min. The distributions of antibody intensities are shown as boxplots. The medians of these distributions were compared using Wilcoxon rank sum test (p-values).

See also Suppl. Fig. S6.

Fig 1

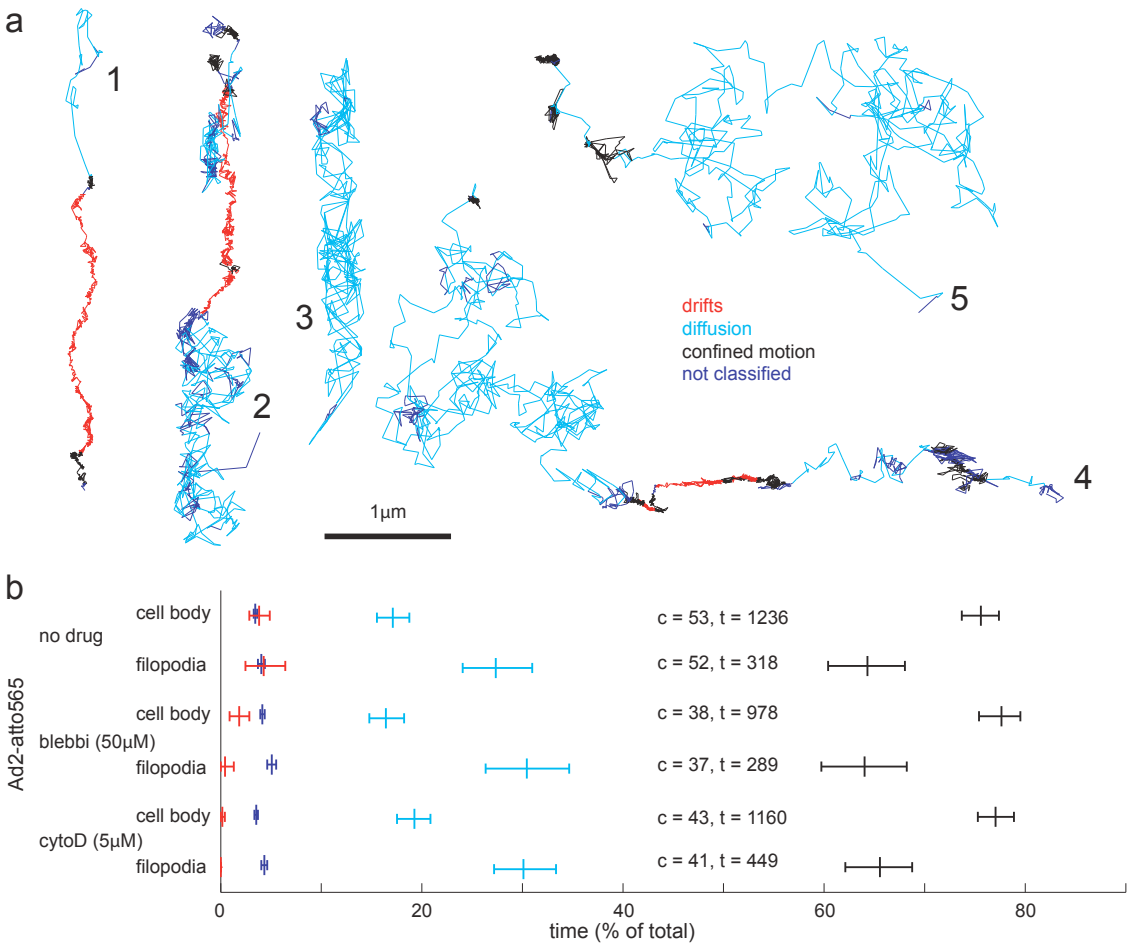
a
1
2
3
4
5
drifts
diffusion
confined motion
not classified
1µm
b
Ad2-atto565
no drug
cell body
filopodia
blebbi (50µM)
cell body
filopodia
cytoD (5µM)
cell body
filopodia
c = 53, t = 1236
c = 52, t = 318
c = 38, t = 978
c = 37, t = 289
c = 43, t = 1160
c = 41, t = 449
0
20
40
60
80
time (% of total)

Fig 2

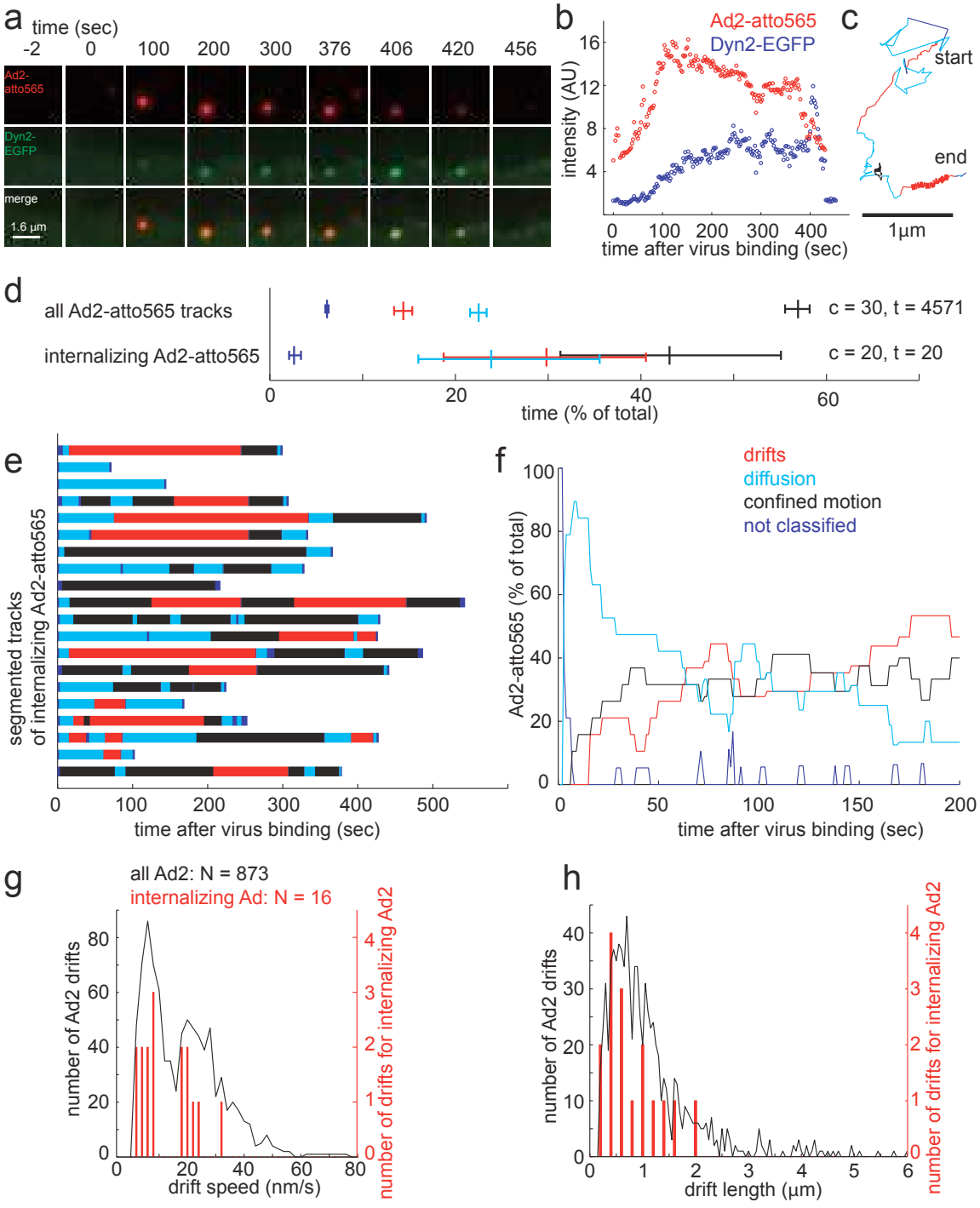
a
time (sec)
-2
0
100
200
300
376
406
420
456
Ad2-atto565
Dyn2-EGFP
merge
1.6 µm
b
Ad2-atto565
Dyn2-EGFP
intensity (AU)
time after virus binding (sec)
c
start
end
1µm
d
all Ad2-atto565 tracks
internalizing Ad2-atto565
c = 30, t = 4571
c = 20, t = 20
time (% of total)
e
segmented tracks of internalizing Ad2-atto565
time after virus binding (sec)
f
drifts
diffusion
confined motion
not classified
Ad2-atto565 (% of total)
time after virus binding (sec)
g
all Ad2: N = 873
internalizing Ad: N = 16
number of Ad2 drifts
number of drifts for internalizing Ad2
drift speed (nm/s)
h
number of Ad2 drifts
number of drifts for internalizing Ad2
drift length (µm)

Fig 3

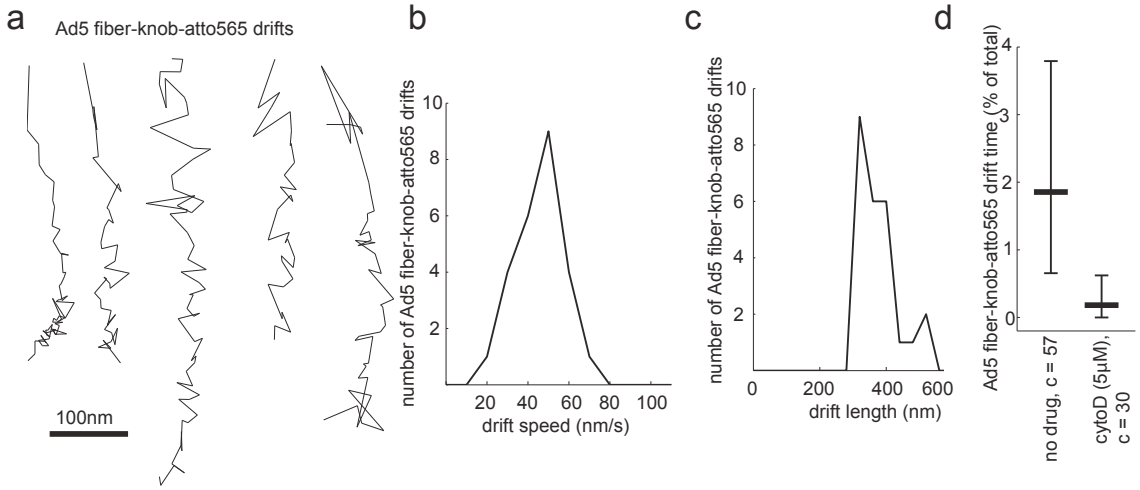
a
Ad5 fiber-knob-atto565 drifts
100nm
b
number of Ad5 fiber-knob-atto565 drifts
drift speed (nm/s)
c
number of Ad5 fiber-knob-atto565 drifts
drift length (nm)
d
Ad5 fiber-knob-atto565 drift time (% of total)
no drug, c = 57
cytoD (5µM), c = 30

Fig 4

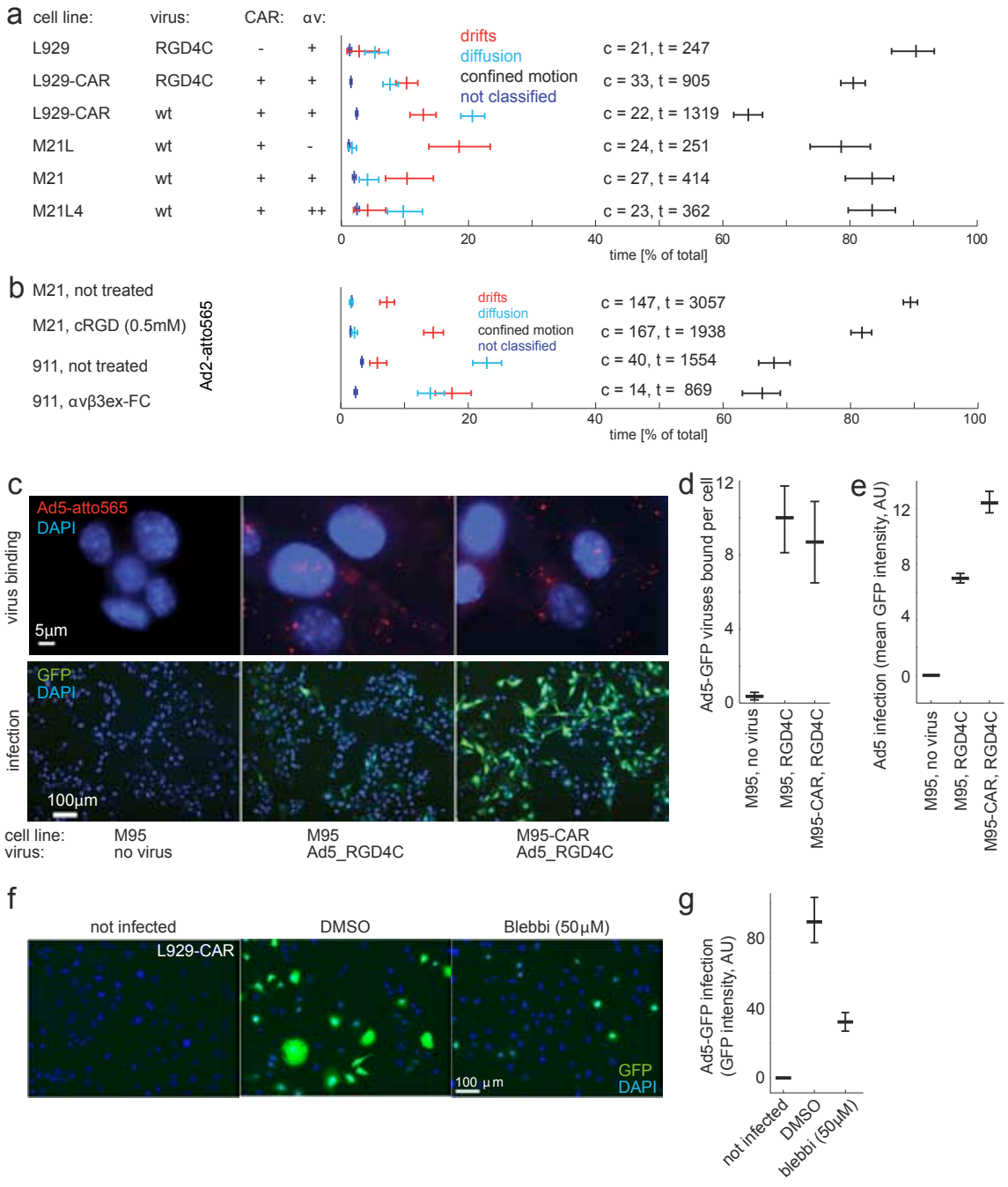
a
cell line:
virus:
CAR:
αv:
L929 RGD4C - +
L929-CAR RGD4C + +
L929-CAR wt + +
M21L wt + -
M21 wt + +
M21L4 wt + ++
drifts
diffusion
confined motion
not classified
c = 21, t = 247
c = 33, t = 905
c = 22, t = 1319
c = 24, t = 251
c = 27, t = 414
c = 23, t = 362
0 20 40 60 80 100
time [% of total]
b
M21, not treated
M21, cRGD (0.5mM)
911, not treated
911, αvβ3ex-FC
Ad2-atto565
drifts
diffusion
confined motion
not classified
c = 147, t = 3057
c = 167, t = 1938
c = 40, t = 1554
c = 14, t = 869
0 20 40 60 80 100
time [% of total]
c
virus binding
Ad5-atto565
DAPI
5µm
infection
GFP
DAPI
100µm
cell line: M95 M95 M95-CAR
virus: no virus Ad5_RGD4C Ad5_RGD4C
d
Ad5-GFP viruses bound per cell
0 4 8 12
M95, no virus
M95, RGD4C
M95-CAR, RGD4C
e
Ad5 infection (mean GFP intensity, AU)
0 4 8 12
M95, no virus
M95, RGD4C
M95-CAR, RGD4C
f
not infected
DMSO
Blebbi (50µM)
L929-CAR
100 µm
GFP
DAPI
g
Ad5-GFP infection (GFP intensity, AU)
0 40 80
not infected
DMSO
blebbi (50µM)

Fig 5

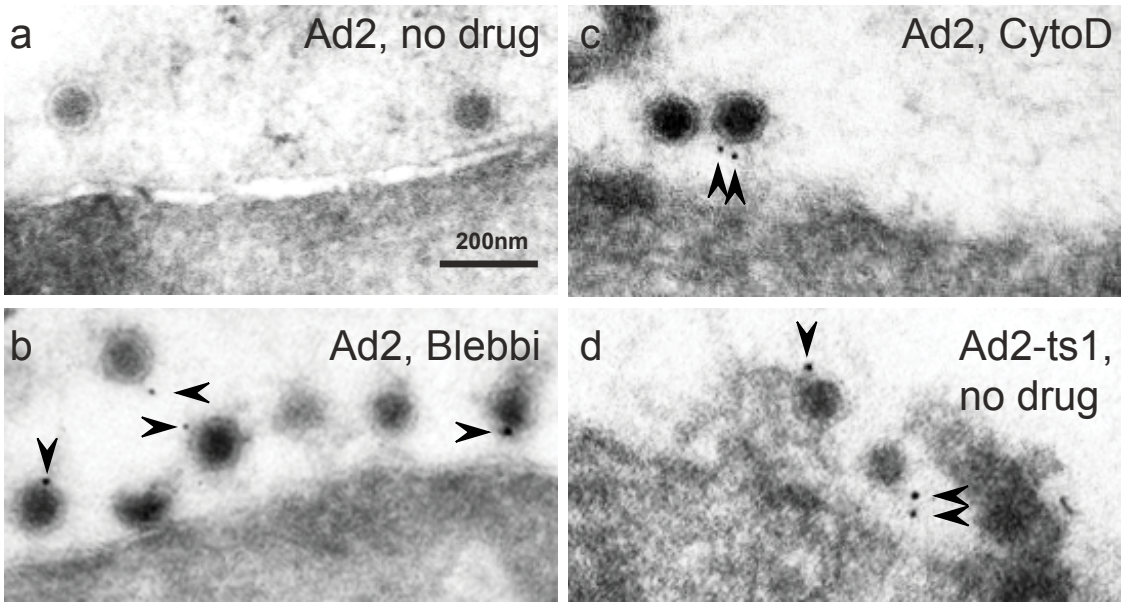

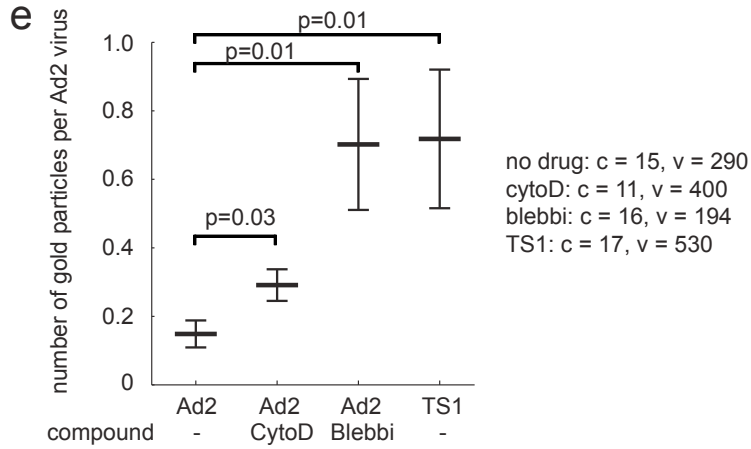

no drug: c = 15, v = 290
cytoD: c = 11, v = 400
blebbi: c = 16, v = 194
TS1: c = 17, v = 530

Fig 6

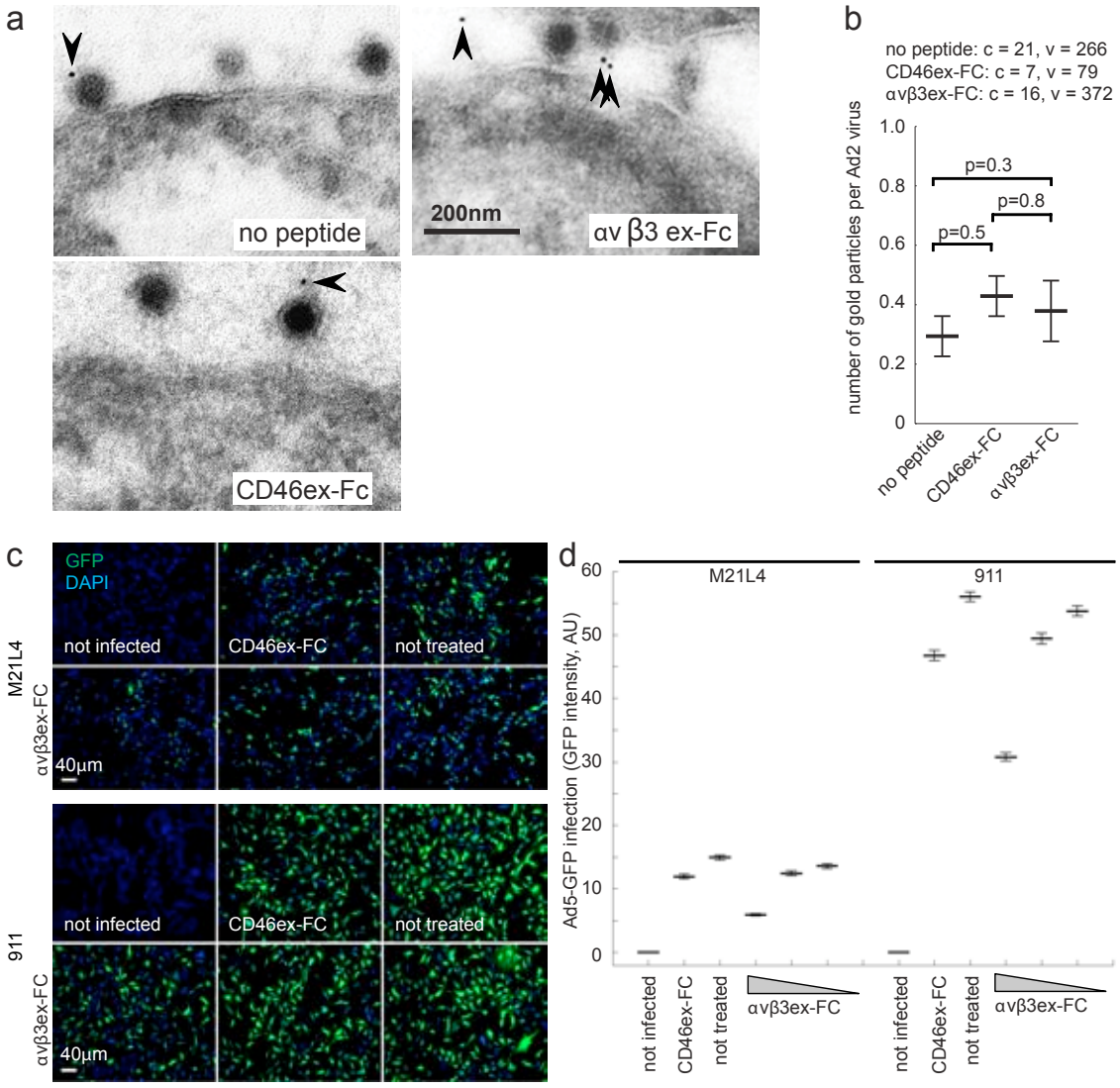
a
no peptide
200nm
αv β3 ex-Fc
CD46ex-Fc
b
no peptide: c = 21, v = 266
CD46ex-FC: c = 7, v = 79
αvβ3ex-FC: c = 16, v = 372
number of gold particles per Ad2 virus
1.0
0.8
0.6
0.4
0.2
0
p=0.3
p=0.8
p=0.5
no peptide
CD46ex-FC
αvβ3ex-FC
c
GFP
DAPI
M21L4
αvβ3ex-FC
not infected
CD46ex-FC
not treated
40μm
911
αvβ3ex-FC
not infected
CD46ex-FC
not treated
40μm
d
M21L4
911
Ad5-GFP infection (GFP intensity, AU)
60
50
40
30
20
10
0
not infected
CD46ex-FC
not treated
αvβ3ex-FC
not infected
CD46ex-FC
not treated
αvβ3ex-FC

Fig 7

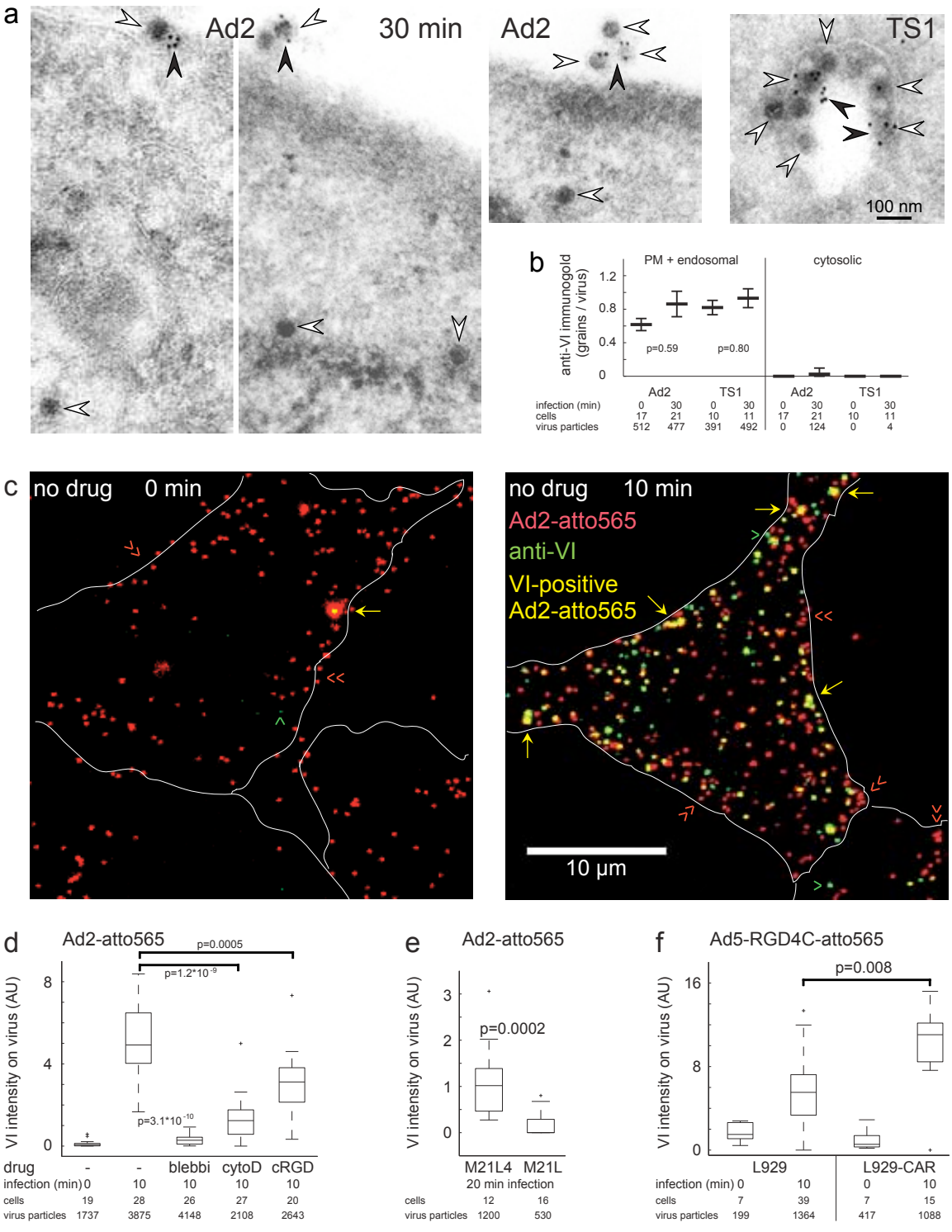
a
Ad2
30 min
Ad2
TS1
100 nm
b
PM + endosomal
cytosolic
anti-VI immunogold (grains / virus)
p=0.59
p=0.80
Ad2
TS1
Ad2
TS1
infection (min) 0 30 0 30 0 30 0 30
cells 17 21 10 11 17 21 10 11
virus particles 512 477 391 492 0 124 0 4
c
no drug 0 min
no drug 10 min
Ad2-atto565
anti-VI
VI-positive Ad2-atto565
10 µm
d
Ad2-atto565
p=0.0005
p=1.2*10-9
p=3.1*10-10
VI intensity on virus (AU)
drug - - blebbi cytoD cRGD
infection (min) 0 10 10 10 10
cells 19 28 26 27 20
virus particles 1737 3875 4148 2108 2643
e
Ad2-atto565
p=0.0002
VI intensity on virus (AU)
M21L4 M21L
20 min infection
cells 12 16
virus particles 1200 530
f
Ad5-RGD4C-atto565
p=0.008
VI intensity on virus (AU)
L929
L929-CAR
infection (min) 0 10 0 10
cells 7 39 7 15
virus particles 199 1364 417 1088

Table of Supplemental Information Contents

Supplemental Information

Supplemental Figures and Figure legends

Supplemental Fig. S1: Characterization of adenovirus movements on the plasma membrane (related to Fig. 1).

A: Acid quenching of extracellular dual labelled Ad2-atto565-FITC.

(**a**) The fluorescence micrographs show quenching of acid-sensitive FITC but not acid-insensitive atto565 fluorescence of viruses at the cell surface whereas intracellular FITC labeled virus particles are acid resistant. Scale bar = 1 µm. (**b**) Intensity profiles of FITC fluorescence from viruses where the signal was quenched are plotted in red, and one acid resistant virus plotted in blue. This experiment reveals that most viruses are extracellular at 5 min post infection, consistent with earlier bulk measurements using radiolabeled Ad2 (Greber et al., 1993).

B: Population properties of entire trajectories and trajectory segments from virus particles on the cell surface.

(**a-c**) Distribution profiles of MSS (moment scaling spectrum) slope, diffusion constant D, run distance, size, and duration for the entire Ad2-atto565 trajectories on L929-CAR cells (overall 1319 Ad2-atto565 trajectories on 22 cells, see main text, Fig. 4a). The plot shows that entire trajectories with MSS slopes < 0.1 were filtered. These immobile particles could not be distinguished from cover glass bound viruses, as described before (Helmuth et al., 2007). The number of events is color-coded and range from 1 (blue) to 12 (red). The same analyses were performed for the confined motions (**d-f**), the drifts (**g-i**), the diffusions (**j-l**) and the not classified motions (**m-o**). For MSS slope / D plots, only segments with more than 50 steps were analyzed. For assessment of the directionality the distance between the first step and the last step of the trajectory or segment was measured and plotted against the size of the trajectory. The size of trajectories and segments was measured in x and y direction and the larger value was chosen. The duration of tracks and segments was analyzed (**c**, **f**, **i**, **l**, **o**). The entire virus trajectories typically lasted less than 100 s (**c**). Reasons for trajectories to terminate include, virus internalization, out of focus motion, or merging of different Ad2-atto565 signals into one single point source of fluorescence. The analysis of the

duration of trajectories revealed that drifts were long lasting (**i**), while the other motion patterns mostly lasted only a couple of seconds (**f**, **l**, **o**). c = number of cells; t = number of trajectories; s = number of segments.

C: Ad2-atto565 drifts have similar speeds and lengths on filopodia and cell body, and are cytochalasin D and blebbistatin dependent but not nocodazole (microtubule)-dependent.

(**a-b**) Segments of Ad2-atto565 drifts on HER-911 cells stably expressing actin-EGFP were analyzed. The drifts were manually classified as cell body or filopodia based, respectively. Distribution of drift speeds (a) and drift lengths (b) for viruses bound to the cell body or filopodia. N = number of drifts.

(**c**) Ad2-atto565 was added to M21 cells and movies were recorded during the first hour of infection. Viruses were continuously binding during this time. Cells were pretreated with 50μM Nocodazole (noc, Sigma), 5 μM CytochalasinD (cytoD) or 50 μM blebbistatin (blebbi) for 20 min, and the drugs were present throughout the experiment. Virus trajectories were obtained by single particle tracking and segmentation. Virus motion was classified as drifts (red), diffusion (cyan), confined motion (black) and not classified (blue). The median time of viruses in each motion type and 95% confidence intervals were obtained by bootstrapping. c = number of cells recorded, t = number of analyzed trajectories.

Supplemental Fig. S1:
Characterization of adenovirus movements on the plasma membrane

A: Acid quenching of extracellular virus

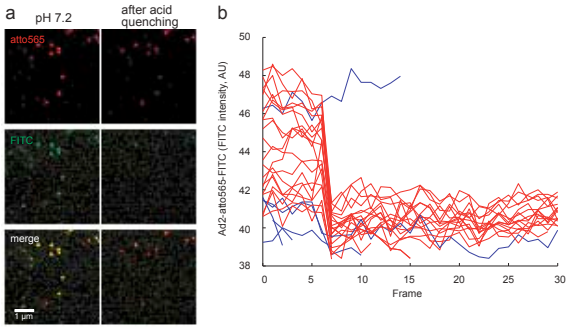

B: Properties of tracks and segments

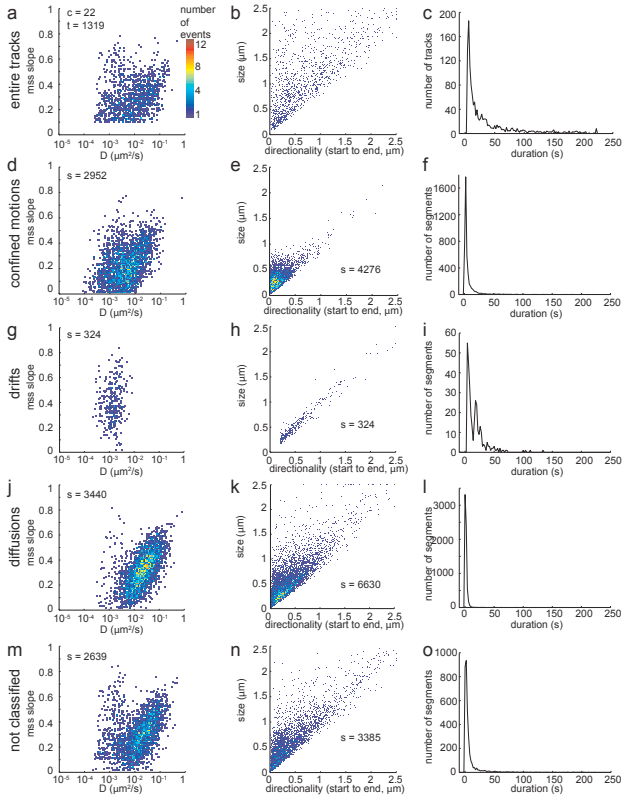

C: Ad2-atto565 drifts on filopodia or cell body have similar speeds & lengths and are actin & myosin-2 dependent but microtubule independent

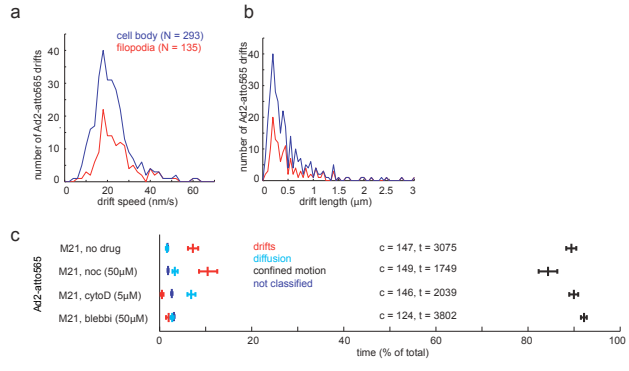

Supplemental Fig. S2: Mean intensity profiles of Ad2-atto565 undergoing internalization in HER-911 cells expressing dynamin2-EGFP (related to Fig. 2).

The virus trajectories (red trace) are aligned at their peak dynamin2-EGFP signal (blue) and the signal intensities were normalized. Standard deviation boundaries from 20 intensity traces are shown as dotted lines. The time indicated is relative to the peak dynamin2-EGFP signal (t = 0). For experimental details see Fig. 1 in main text.

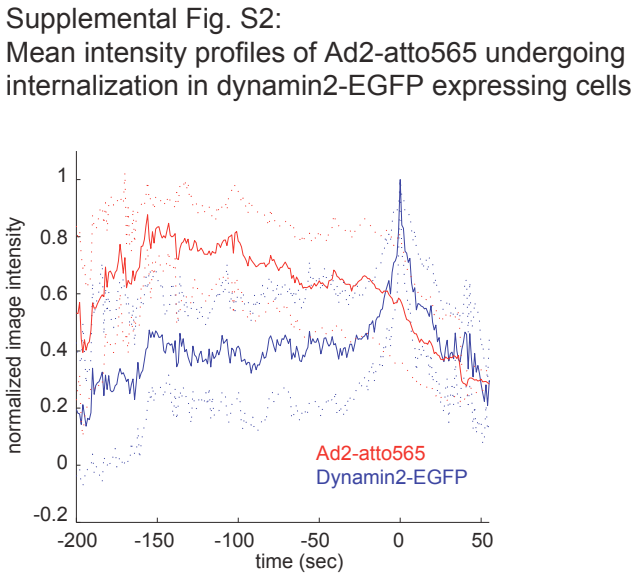

Supplemental Fig. S3: CAR mediates diffusive motions of Ad5 fiber-knob (related to Fig. 3).

(**a**) SDS-PAGE of His-tagged fiber knob. Ad5-fiber-knob was expressed in SF9 insect cells and purified on Ni-NTA-agarose, labeled with atto565 as described for labeling Ad2, fractionated by SDS-PAGE, and stained with Coomassie brilliant Blue. Molecular weight markers (PageRuler Plus pre-stained protein ladder, Fermentas) are indicated in relative kDa (Mr).

(**b-c**) FRAP curves of L929 cells transiently expressing GFP-CAR in the absence (dark blue) or in presence of Ad5 fiber-knob (light blue). The data points are the means +/- SEM from 11 cells each. (**c**) Means including SEM of FRAP half recovery times ($T_{1/2}$) obtained from the data shown in b. $p < 0.001$ (Student's-t test).

(**d**) Normalized comparison of the diffusion constants of Ad5 fiber-knob-atto565 trajectories (black) and Ad2-atto565 diffusion segments (blue) obtained by TIRF microscopy and trajectory segmentations on HER-911 cells. c = number of cells, t = number of analyzed trajectories (fiber-knob) or diffusion segments (Ad2).

(**e**) Four example trajectories of Ad5 fiber-knob-atto565 on HER-911 cells collected from the peak regions of the diffusion constant histograms (d). Images were acquired on a TIRF microscope at 25 Hz, and fiber knobs were tracked using the procedure described for Ad2-atto565. The first 10 steps of each trajectory are highlighted in red.

Supplemental Fig. S3:
CAR mediates diffusive motions of Ad5 fiber-knob

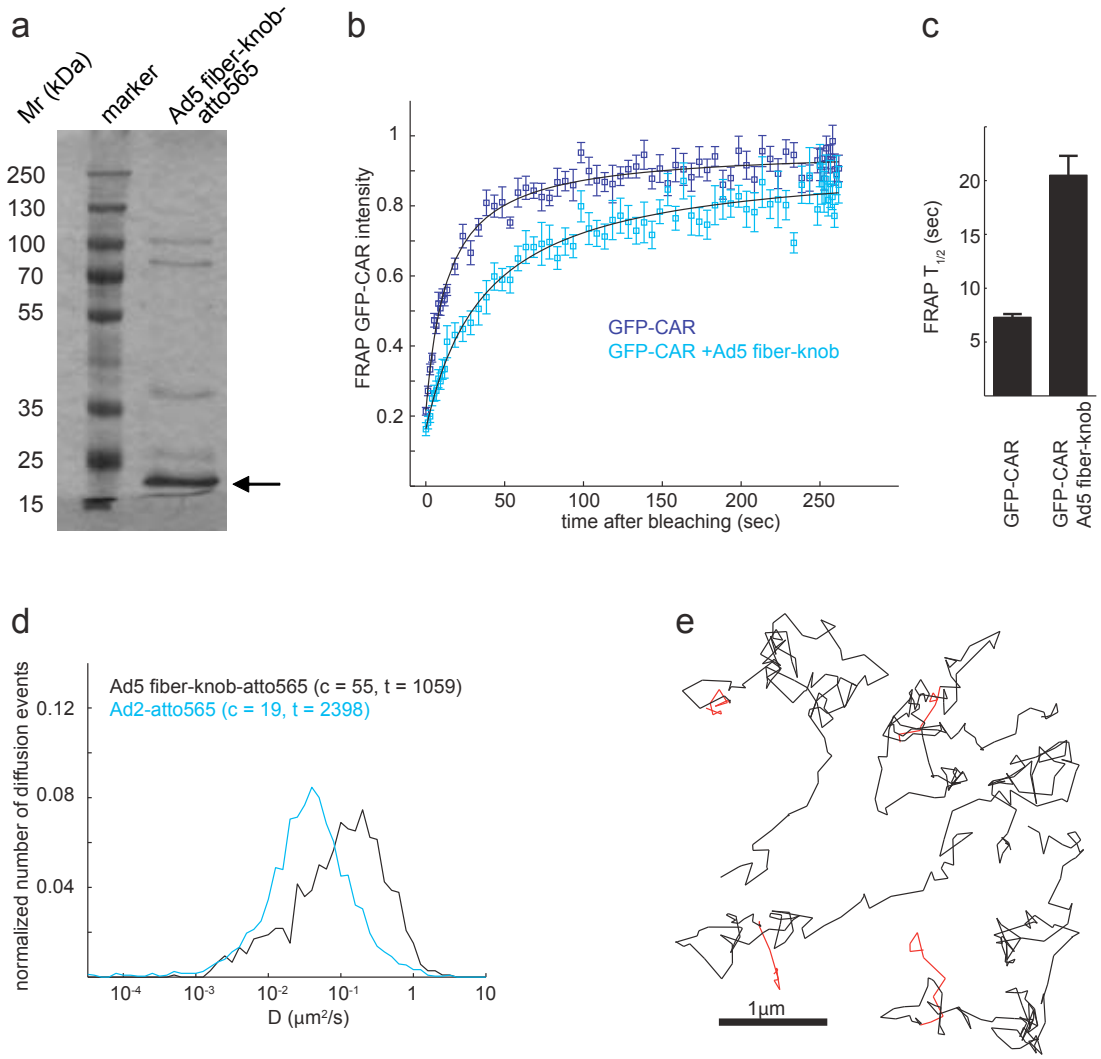

Supplemental Fig. S4: Characterization of adenovirus movements on CAR and integrins, respectively (related to Fig. 4).

A: GPI-linked CAR mediates Ad2-atto565 drifts.

Ad2-atto565 was bound to CAR-negative L929 cells transiently expressing full length CAR (same data as in Fig. 4a), GPI (glycosyl-phosphatidyl-inositol)-anchored extracellular domain of CAR (CAR-GPI) or CAR lacking the cytosolic domain (CAR-tailless). Cells were transfected with the corresponding CAR expression constructs by Polyethylenimine (PEI; linear, Mr 25,000, Polysciences) together with a GFP expression plasmid as reporter for transfection. Movies were recorded during the first 5 minutes after virus addition to cells. Data are represented as described in Supplemental Fig. S1Ac.

B: Integrin-targeted Ad5-RGD4C-atto565 has lower diffusion constants than CAR-targeted Ad5-RGD4C-atto565 or Ad5-atto565.

Comparison of the diffusion constants (D) of Ad5-RGD4C-atto565 on L929 cells (light blue, CAR negative), or Ad5-RGD4C-atto565 (dark blue) and Ad2-atto565 (red) on L929-CAR cells (CAR expressing) from normalized histograms. The diffusion constants were obtained from the trajectory segments classified as diffusion in the experiment presented in Fig 4a. c = number of cells, s = number of diffusion segments.

C: Purified αvβ3ex-Fc bind to Ad2 immobilized on a Biacore chip.

(**a-b**) Purified extracellular domains of αv-Fc and β3-Fc (αvβ3ex-Fc) as well as CARex-Fc and CD46ex-Fc analyzed by Coomassie brilliant Blue stained SDS-PAGE (a), and a Western blot with fractions eluted from ProteinG-Sepharose, stained with an anti-human Fc IgG linked to horse raddish peroxidase is shown in (b).

(**c-e**) Surface plasmon resonance (SPR) analysis of immobilized Ad2 probed with different concentrations of soluble integrins (c), soluble extracellular CAR (CARex-Fc, Ebbinghaus et al., 2001) (d) or soluble CD46ex-Fc (Sirena et al., 2004) (e). Note that αvβ3ex-Fc was observed to bind Ad2, albeit at higher protein concentrations than the high affinity binder CAR, while CD46ex-Fc did not bind.

Supplemental Fig. S4:
Characterization of adenovirus movements on CAR and integrins, respectively

A. GPI-linked CAR mediates Ad2-atto565 drifts

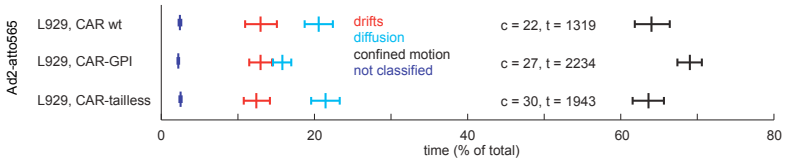

B: Integrin-targeted Ad5-RGD4C-atto565 has lower diffusion constants than CAR-targeted Ad5-RGD4C-atto565 or Ad5-atto565

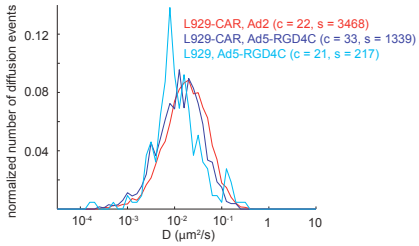

C: Purified αvβ3ex-Fc binds to Ad2 immobilized on a Biacore chip

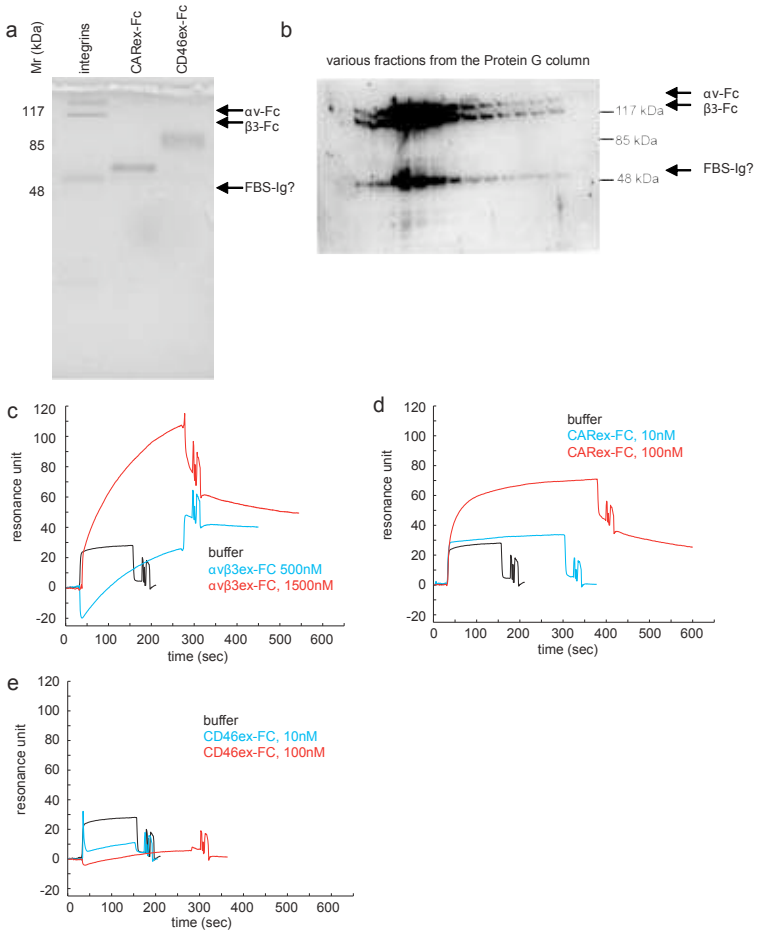

Supplemental Fig. S5: Shedding of fibers from incoming Ad2 requires acto-myosin mediated drifts and alpha v integrins (related to Fig. 5).

(**a**) HeLa cells treated with or without drugs were inoculated with Ad2-atto565 by cold synchronization, warmed as indicated, fixed and stained for fiber with R72 antibody and DAPI, imaged by confocal microscopy, processed and analyzed as indicated in Supplemental Procedures. Panel (**b**) shows the distributions of antibody intensities as boxplots. The medians of these distributions were compared using Wilcoxon rank sum test (p-values).

(**c,d**) Human melanoma M21L (lacking alpha v integrin) and M21L4 (positive for alpha v integrin) cells were inoculated with Ad2-atto565 at 37°C for 20 min, and processed and analyzed as described in panels (a,b).

Supplemental Fig. S5:
Shedding of fibers from incoming Ad2 requires acto-myosin mediated drifts and alpha v integrins

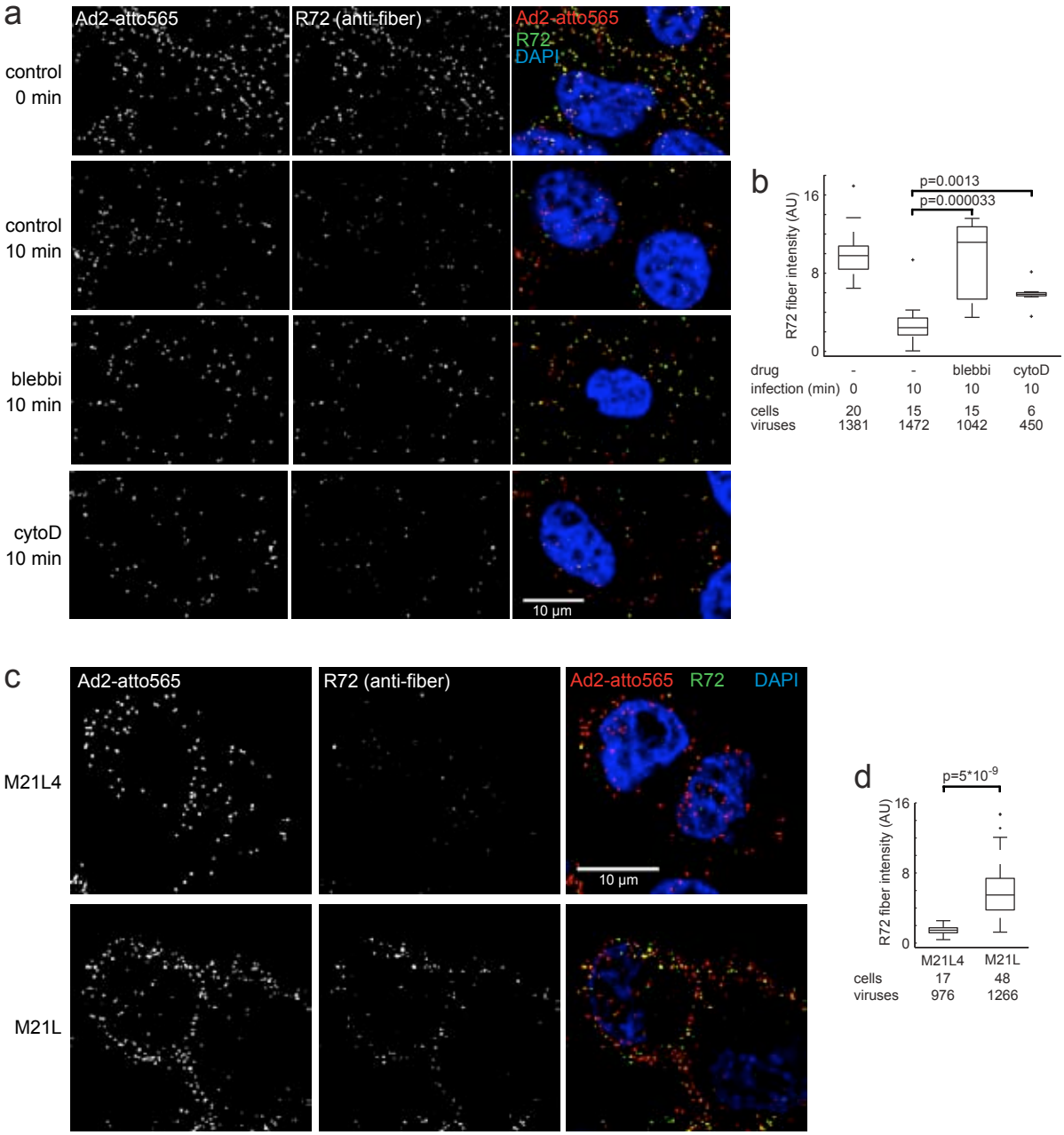

Supplemental Fig. S6: CAR drifts and integrins trigger adenovirus uncoating (related to Fig. 7).

A: Native cell-free Ad2 exposes fiber (R72), but not protein VI epitopes.

(**a,b**) Purified native Ad2-atto565 bound to cover glass reacts with the R72 but not anti-protein VI antibody. Confocal fluorescence microscopy images were acquired and processed as described in Supplemental Procedures. (**b**) X-Y plots of virus intensity (atto565) versus fiber or protein VI intensity (revealed by an anti-rabbit-atto488 secondary antibody). The plot reveals a heterogeneity of fiber staining on purified Ad2-atto565. Each circle represents an individual virus particle.

(**c**) SDS-PAGE and Western blots against Ad2 indicate that the rabbit R72 and anti-protein VI antibodies recognize Ad2 fiber and protein VI, respectively.

(**d**) Analysis of purified Ad2 and TS1 used for the cryo-section immuno-EM. The results show that there are very low levels of broken protein VI positive particles. The experiment was conducted and plotted as described for panel b, except that viral particles were identified by 6A4 labeling of fibers, followed by secondary anti-mouse-alexa594.

B: Transient appearance of protein VI epitopes on incoming Ad2 requires acto-myosin mediated drifts and alpha v integrins.

(**a**) The peak of protein VI exposure on incoming Ad2-atto565 occurs at 10 min post warming in cold-synchronized HeLa cell infections. Distributions of anti-protein VI antibody intensities are shown as boxplots with medians. Comparison by Wilcoxon rank sum test (p-values).

(**b**) The exposure of protein VI epitopes requires acto-myosin mediated drifts. HeLa cells were treated or not treated with drugs as indicated, and processed for confocal fluorescence microscopy as described in Supplemental Procedures. Please note that the images shown for 0min and 10min of control (no drug) cells are the same as shown in Fig.7.

C: Enhanced exposure of protein VI on Ad2-atto565 in alpha v integrin-positive M21L4 cells compared to alpha v integrin-lacking M21L cells.

M21L and M21L4 cells were inoculated with Ad2-atto565 for 20 min at 37°C, fixed, processed for staining of protein VI and imaged as described in Supplemental Procedures.

D: CAR supports exposure of protein VI epitopes on incoming Ad5.

L929 and L929-CAR cells were inoculated with Ad5-RGD4C-atto565 by cold synchronization and warmed for 0 or 10 min as indicated, fixed, processed for staining of protein VI and imaged as described in Supplemental Procedures.

Supplemental Fig. S6: CAR drifts and integrins trigger adenovirus uncoating

A: Cell-free Ad2 or TS1 expose fiber (R72), but not protein VI epitopes

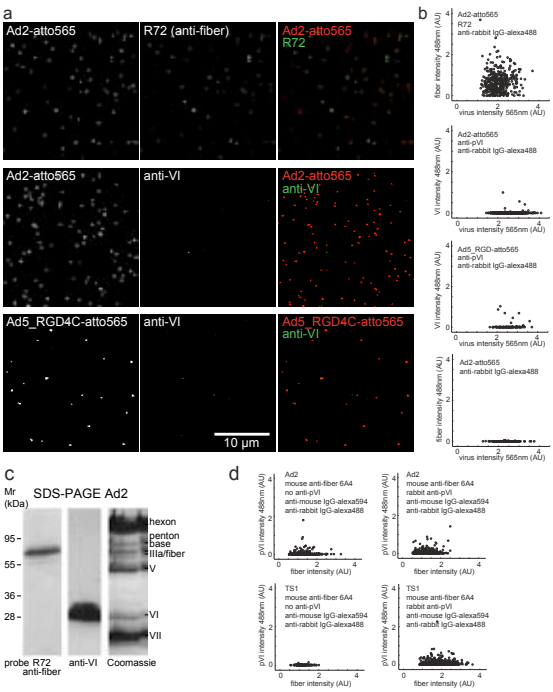

B: Transient appearance of protein VI epitopes on incoming Ad2 requires acto-myosin mediated drifts and alpha v integrins

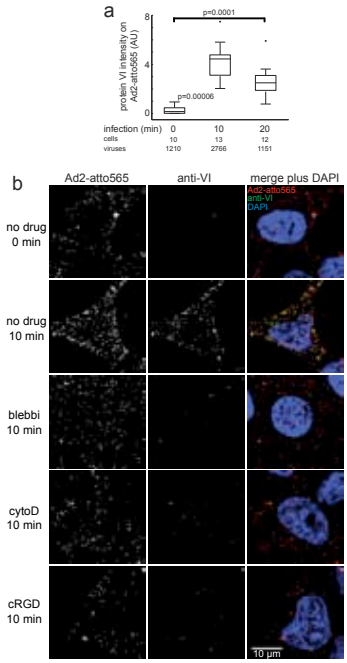

C: Enhanced exposure of protein VI on Ad2-atto565 in alpha v integrin-positive M21L4 cells compared to alpha v integrin-lacking M21L cells

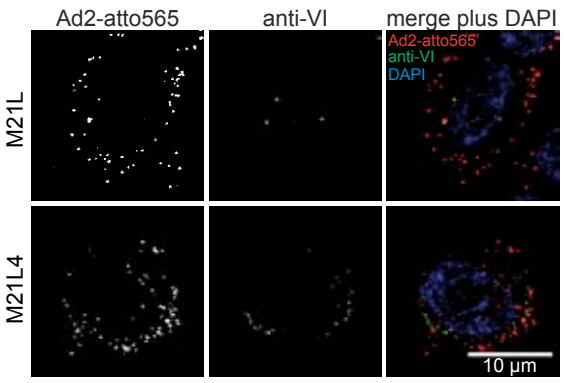

D: CAR supports exposure of protein VI epitopes on incoming Ad5

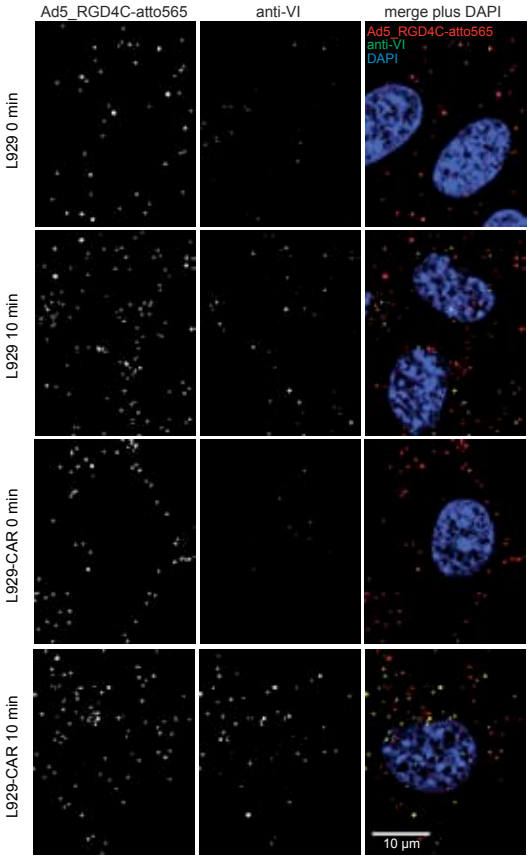

Supplemental Fig. S7: Model for how receptor-mediated motions of human adenovirus trigger viral uncoating and protein VI activation.

Immediately after binding to the surface, adenovirus diffuses on CAR for many seconds (step 1). This motion allows rapid scanning over large areas of plasma membrane. The diffusive motions become less frequent with prolonged surface residence before virus internalization. Decreased diffusion coincides with increasing drifting and confined motions (step 2). Clustering of CAR triggers CAR drifts that are driven by dynamic actin filament turnover and the action of myo2. Drifting CAR receptors together with immobile integrins induce fiber shedding (step 3). This may occur by virus drifts (3a) or by fiber drifts (3b). Integrin binding to penton base may induce conformational changes, which further weaken the interaction between the capsid and the penton-fiber complex. During of subsequent to dynamin-mediated endocytosis, protein VI is exposed from the capsid (step 4). Although fiber-shedding is linked to protein VI exposure, it is presently unclear if protein VI is exposed through the destabilized vertices or other breaches in the capsid structure. Capsid uncoating may be further enhanced by the release of minor capsid stabilizing proteins, such as the zippering protein IIIa, which connects neighboring hexons, or the internal protein VIII. For details, please refer to the discussion in the main text.

Supplemental Fig. S7:
Model for how adenovirus receptor movements trigger virus uncoating

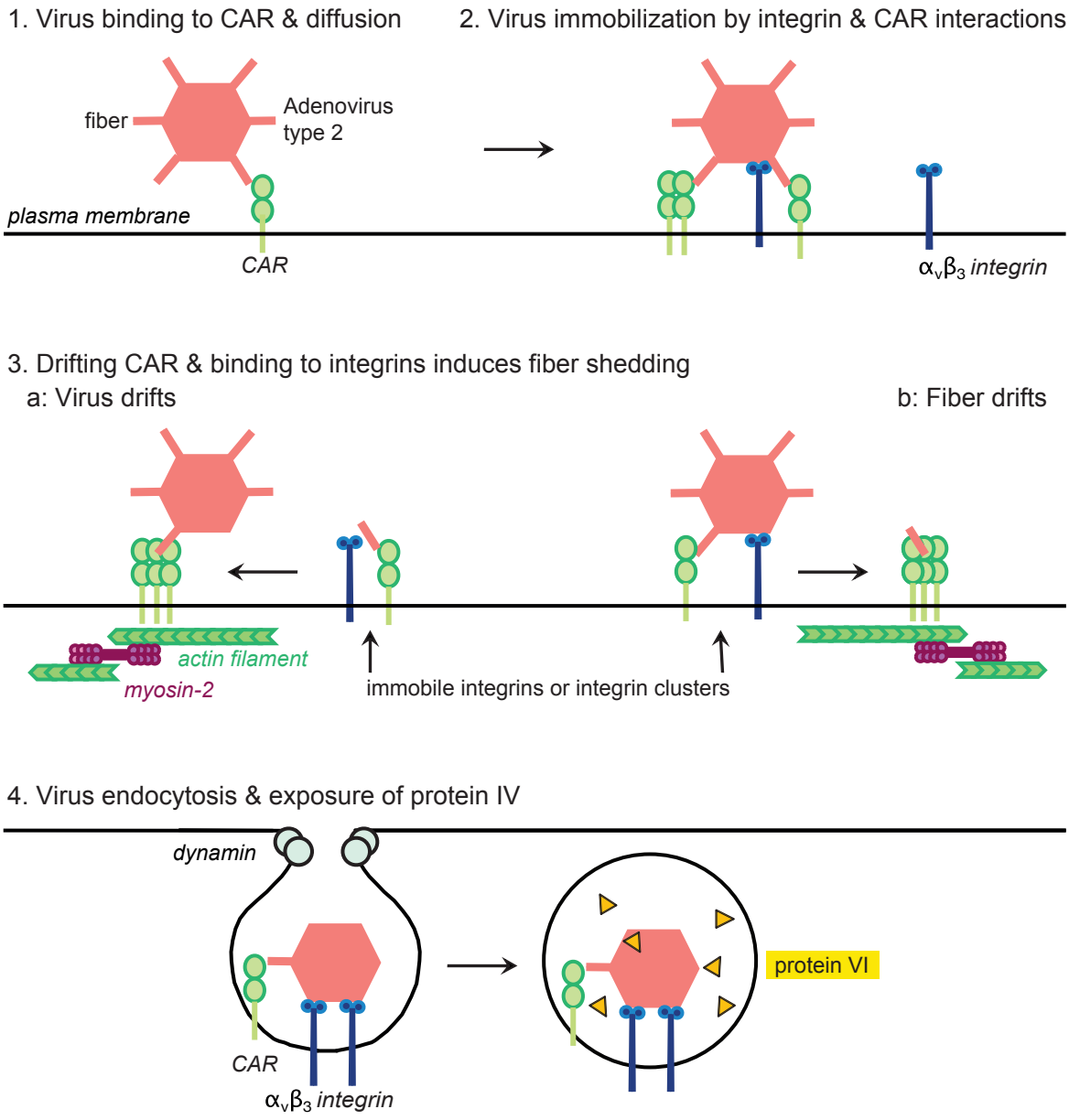

Supplemental Movie 1: Heterogeneous movements of Ad2-atto565 on filopodia of HER-911 cells (related to Fig. 1).

Ad2-atto565 was observed on elongated cell extensions (filopodia) of HER-911 cells stably expressing actin-EGFP. Images were recorded on a spinning disc confocal microscope at 25 Hz during the first 5 min after virus addition. These data reveal the heterogeneous trajectories on filopodia.

Supplemental movie 1 (still image):
Heterogeneous viral motions on filopodia of HER 911 cells

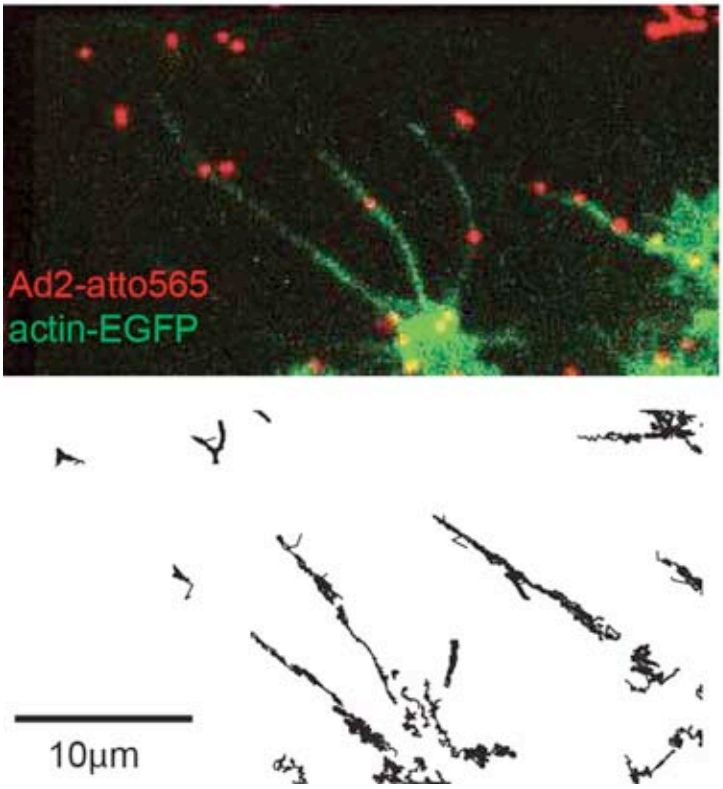

Supplemental Movie 2: Heterogeneous movements of Ad2-atto565 on the HER-911 cell body (related to Fig. 1).

Ad2-atto565 was observed on the cell body of HER-911 cells stably expressing actin-EGFP. Images were recorded on a spinning disc confocal microscope at 25 Hz during the first 5 min after virus addition. These data reveal the heterogeneous trajectories on the cell body.

Supplemental movie 2 (still image):
Heterogeneous viral motions on the body of HER 911 cells

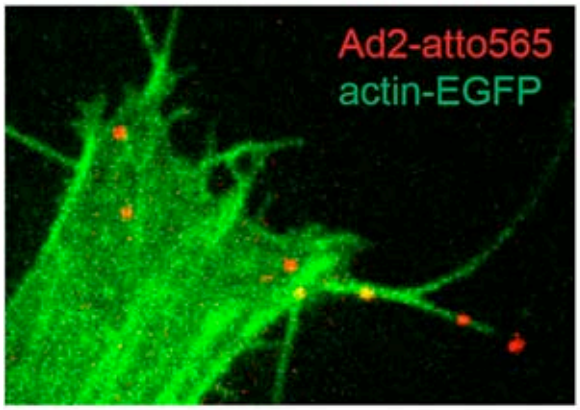

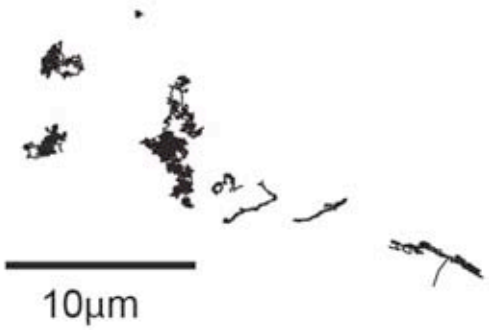

Supplemental Movie 3: Internalization of fluorescent Ad2-atto565 imaged by TIRF microscopy (related to Fig. 2).

Ad2-atto565 was added to HER-911 cells expressing dynamin2-EGFP and immediately thereafter recorded by TIRF microscopy for 10 min at 1 Hz in the red (568nm) and 0.5 Hz in the green channel (488nm). Virus internalization events where Ad2-atto565 particles disappeared from the TIRF view simultaneously with a dynamin2-EGFP blink were manually selected (see also Fig. 2a-c). Scale bar 1.6 µm.

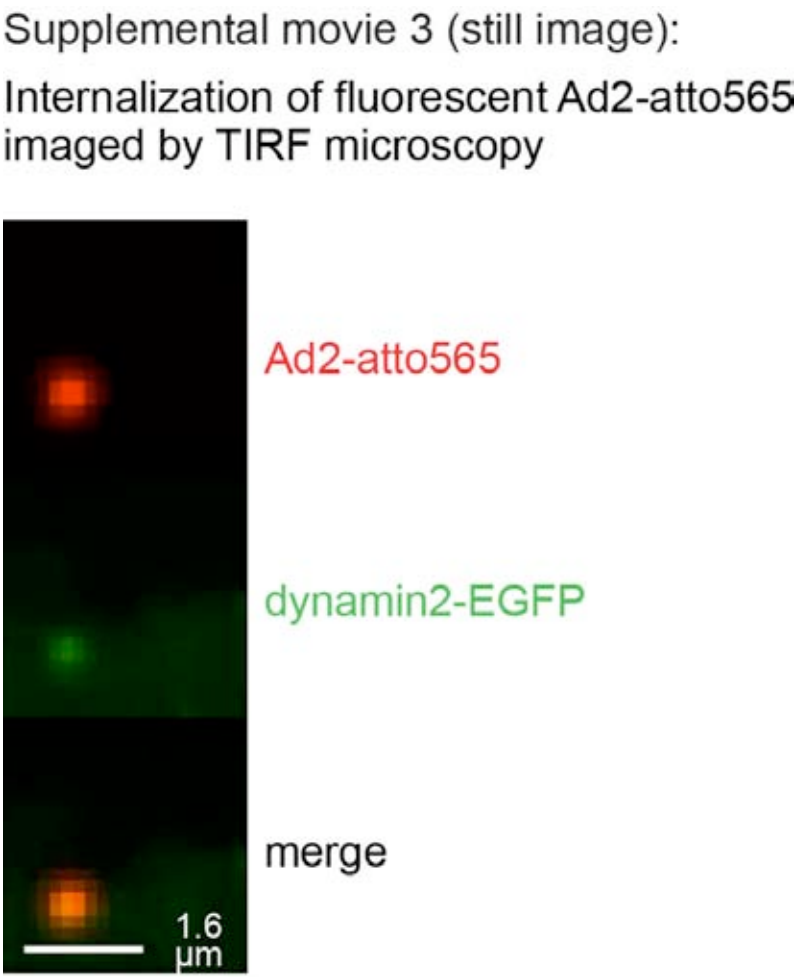

Supplemental Experimental Procedures

Cells and viruses

Human melanoma M21, M21 and M21L cells, obtained from Dr. D. Cheresh (Scripps Research Institute, La Jolla, USA), were grown in RPMI 1640 plus 10% fetal bovine serum (Gibco) and 1% non-essential amino acids (Sigma, Buchs, Switzerland). Human embryonic retinoblast 911 cells obtained from Dr. A. van der Eb (University of Leiden, The Netherlands), mouse fibrosarcoma L929, L929-CAR, human melanoma M950710 and M950710-CAR were grown in DMEM plus 10% fetal bovine serum and 1% non-essential amino acids. HER-911 cells stably expressing EGFP-actin or dynamin2-EGFP were transfected with the plasmid encoding the fusion proteins and sorted using a FACS-Aria cell-sorting system (Becton Dickinson). Ad2 and Ad5, Ad5-RGD4C, Ad5-GFP and TS1 were grown, isolated, and labeled with atto565 (Atto-tec, Germany) as described (Suomalainen et al., 1999). Ad2 and Ad5 are closely related and have been used interchangeably in cell biological experiments and gene therapy applications (Imelli et al., 2009; Volpers and Kochanek, 2004).

Acid quenching of dual color Ad2-atto565-FITC

Ad2 was labeled with equal amounts of atto565 and FITC (Ad2-atto565-FITC) and added to human M21 cells on a TIRF microscope, incubated at 37°C in HANKS buffered saline for 5 min (or up to 10 min, not shown), and acidified with 20 mM sodium citrate, pH 4.5, 0.15 M NaCl. FITC is a pH-sensitive fluorophore, which is strongly quenched below pH 5 due to protonation (Sjoback et al., 1988). Atto565 is covalently linked specifically to the hexon protein of Ad2 virions (data not shown).

Infection analyses

Cells were grown in 96 well plates one day before infection, pretreated with drugs, DMSO carrier or proteins for 1 h, infected with Ad5-GFP or Ad5-RGD4C-GFP expressing GFP from the E1A region. Cells were fixed with paraformaldehyde (Sigma) 12h post infection, and stained with DAPI (Sigma). Images were acquired on an ImageXpress Micro (Molecular Devices) automated microscope equipped with a CoolSNAP HQ camera (Roper Scientific), a 10x SuperFluor (N.A. 0.5) objective

(Nikon) and controlled by Metamorph. A custom programmed Matlab (The Mathworks) routine recognized the DAPI stained nuclei and quantified the GFP signal over this area of the cell. The background fluorescence intensity was obtained from uninfected cells. To quantify virus binding the images were recorded with a 40x SuperFLuor (N.A. 0.95) objective (Nikon) on the same microscope and viruses detected as described for the particle tracking (Sbalzarini and Koumoutsakos, 2005).

Virus endocytosis

L929 or L929-CAR cells grown on Alcian blue-coated coverslips were incubated with Ad5-RGD4C-atto565 in RPMI-0.2% BSA medium at 0°C for 60 min, as described above for the protein VI stain. Since penton base-integrin interaction is of lower affinity than fiber-CAR interaction, 100-fold more virus was used in the L929 inoculum than in the L929-CAR one. After cold binding, cells were warmed to 37°C for 0 min or 10 min. Afterwards cells were placed on ice and incubated for 60 min with the mouse anti-hexon 9C12 antibody diluted in RPMI-BSA (this antibody was developed by Laurence Fayadat-Dilman and Wiebe Olijve, and was obtained from Developmental Studies Hybridoma Bank, University of Iowa). After extensive washing, cells were fixed with 3% paraformaldehyde, quenched, permeabilized and stained with Alexa Fluor 680-conjugated goat anti-mouse antibodies (Molecular Probes, Invitrogen) and imaged as described for anti-fiber staining. A Matlab-based routine (Puntener et al., 2011) was used to determine the 9C12 signal on virus particles and viruses negative for 9C12 were scored as endocytozed particles.

Immunofluorescence assay for fiber release

Hela cells (from ATCC) on Alcian blue-coated coverslips in 24-well dishes were pretreated with DMSO or 50 µ M blebbistatin or 5 µ M cytoD for 30 min in DMEM supplemented with 0.2% BSA. Ad2-atto565 diluted in RPMI-0.2% BSA (0.4 µg, 0.1 µg or 0.15 µg per well for DMSO, blebbistatin or cytochalasinD treated cells, respectively) was bound to cells at 0°C for 60 min in the presence of drugs. Cells were washed with excess RPMI-BSA and incubated in the same medium containing DMSO or the drugs for 0 min or 10 min at 37°C. Cells were subsequently washed with PBS on ice, fixed with 3% paraformaldehyde in PBS for 20 min at RT, quenched for 10 min with 25 mM NH_4Cl in PBS, and permeabilized with 0.5% Triton X-100 in PBS for 5 min at RT. Cells

were blocked with 10% goat serum, and stained against fiber with the R72 anti-fiber antibody (Baum et al., 1972), and AlexaFluor488 goat anti-rabbit antibody (Molecular Probes, Invitrogen). Prior to use the R72 antibody was preadsorbed on fixed and permeabilized, uninfected cells. Images were recorded with an inverted Leica SP2 confocal microscope equipped with 63× (oil immersion, numerical aperture 1.4) objective. Excitations were at 405 nm (DAPI), 488 nm (R72) and 543 nm (Ad2-atto565). Stacks were recorded at 0.5 µm intervals using 4× averaging. Images shown represent maximum projections of individual stacks (R72 and virus) or a single confocal section (DAPI). Fiber release was analyzed in infected M21L and M21L4 cells as described above for HeLa cells, except that cells were seeded on poly-lysine-coated coverslips and cells were infected with 3 µg (M21L) or 2 µg (M21L4) of Ad2-atto565 at 37°C for 20 min.

Immunofluorescence assay for protein VI exposure

Two µg of Ad2-atto565 was used per well to infect HeLa cells, and cRGD peptides (0.2 mM) were added during the last 30 min of cold binding. Cells were fixed after 0 min and 10 min incubation at 37°C. M21L and M21L4 cells were infected with Ad2-atto565 (1.5 µg per well) at 37°C for 20 min. To analyze protein VI exposure in L929 and L929-CAR cells, Ad5-RGD4C-atto565 (2.1 µg/well for L929 and 0.1 µg/well for L929-CAR) was bound to cells at 0°C for 60 min, and virus was subsequently internalized at 37°C for 0 min or 10 min. Cells were stained against protein VI using affinity-purified rabbit polyclonal antiserum and AlexaFluor488 goat anti-rabbit antibodies, and antibody intensity was measured on the position of the virus and plotted against the virus intensity. Image acquisition and processing was done as described for fiber release.

For cell-free virus analyses, Ad2-atto565 or Ad5-RGD4C-atto565 were bound to poly-lysine-coated coverslips, and coverslips stained with R72 or anti-protein VI antiserum, imaged and processed as described for infected cells. The antibody intensity was measured on the position of the virus and plotted against the virus intensity.

Plasmids

EGFP-β-actin under the β actin promotor was obtained from Bernhard Wehrle-Haller, University of Geneva. GFP-CAR (Ebbinghaus et al., 2001) was cloned by PCR

(polymerase chain reaction) amplification of the CAR leader sequence and signal peptide coding region using the 5' oligonucleotide ACCGCTAGCCCAGGAGCGAGAGCCGCC, and the 3' oligonucleotide CGCAAGCTTACTTCTGGCGAAATCCAC, inserted into the pcDNA3.1(+)-neo plasmid (Invitrogen) by the sites Nhe1 and HindIII. Next EGFP (A206K) (Zacharias et al., 2002) was amplified by PCR using the 5' oligonucleotide ACCAAGCTTGTGAGCAAGGGCGAGGAG, and 3' oligonucleotide CGCGGATCCCTTGTACAGCTCGTCCAT, and inserted into the HindIII and BamH1 sites. The CAR coding sequence downstream of the signal peptide was amplified by PCR using 5' oligonucleotide ACCGAATTCTTTGAGTATCACTACTCCTGA, and 3' oligonucleotide CGCTCTAGACTATACTATAGACCCATC, and inserted into the EcoR1 and Xba1 sites. The construct was verified by DNA sequencing.

Chemicals and antibodies

Cytochalasin D and (+/-)blebbistatin (Calbiochem) were dissolved in dimethylsulfoxide (Sigma) and kept in aliquots at -20°C until use. Dissolved blebbistatin was used within 3 weeks, and protected from light inactivation (Sakamoto et al., 2005). cRGD peptide and R72 antibody were used as described (Nakano et al., 2000). Oligonucleotides were obtained from Microsynth (Balgach, Switzerland). The mouse monoclonal anti-fiber antibody 6A4, which recognizes Ad2 but not Ad5 fibers, was obtained from J. Chroboczek (Fender et al., 1995). HRP conjugated rabbit anti-human IgG (Cell Signalling Technology) was used for Western blots.

Recombinant protein VI was used as an antigen to produce polyclonal anti-VI antiserum. cDNA encoding the mature form of protein VI was amplified from Ad2-BAC53 (Hilgendorf et al., 2003) using oligos 5'-ATC CTG GCT AGC GCC TTC AGC TGG GGC TCG C-3' and 5'- ATC TCC GAA TTC TCA CAG ACC CAC GAT GCT GTT CAG -3'. The amplified cDNA was cloned into the NheI and EcoR1 sites of pET28a+ (Novagen), and the inserted DNA was verified by sequencing. Recombinant protein VI was expressed in BL21 (DE3) at 37°C by auto-induction (Studier, 2005). Cells were washed once with PBS and cell pellet was resuspended in Bugbuster protein extraction reagent (Novagen) supplemented with 25 mM Hepes-KOH pH 7.4, 0.3 M NaCl, 0.5 mg/ml lysozyme, 20 µg/ml DNase I and complete mini EDTA-free protease

inhibitor cocktail (Roche Diagnostics GmbH). After 25 minutes on ice, cell debris were pelleted at 16,000 × g for 15 min at 4°C. The supernatant was adjusted to 50 mM imidazole and HIS-tagged protein VI was bound to Ni-NTA agarose (Qiagen). The agarose was washed twice with a buffer containing 20 mM Hepes-KOH pH 7.4, 500 mM NaCl, 50 mM imidazole, 0.1% Triton X-100, once with a buffer containing 20 mM Hepes-KOH pH 7.4, 100 mM NaCl and twice with a buffer containing 40 mM Hepes-KOH pH 7.4, 2 mM ATP, 10 mM $MgSO_4$. Recombinant protein VI was eluted with a buffer containing 750 mM imidazole pH 7, 300 mM NaCl and 0.1% triton X-114, and dialyzed against PBS. Rabbit polyclonal antiserum against the purified recombinant protein VI was produced by BioGenes (Berlin, Germany). Animal work was conducted according to NIH standards controlled by the office of laboratory animal welfare (certificate no A5755-01 for Biogenes, Germany). IgG fraction of the antiserum was used for Western blot analyses and the antiserum was affinity-purified for immunofluorescence. The affinity-purification was done by standard procedures using Ad2-derived protein VI bound to Hybond-P PVDF membrane (GE Healthcare).

SDS-PAGE and Western blots

SDS-PAGE (Supplemental Fig. S10) was done using 12% poly-acrylamide gels and the gel was divided into two parts. One part was stained with Coomassie brilliant blue and proteins in the other part were transferred to Hybond-P PVDF membrane (GE Healthcare). Membranes were stained with the R72 anti-fiber antibody or the anti-protein VI antiserum (IgG fraction), and the primary antibodies were detected using HRP-conjugated secondary anti-rabbit antibodies (Cell Signalling Technology) and the ECL plus Western blotting detection kit (GE Healthcare).

Proteins

His-tagged Ad5-fiber knob was expressed and purified by Ni-NTA agarose, labeled with atto565, purified by ion-exchange column and eluted with NaCl. Expression plasmids for soluble αv and β3 integrins tagged with human Fc (1222 amino acids for the mature αv-Fc fusion protein, calculated molecular weight of 135 kDa, and 948 amino acids for the β3-Fc, 105 kDa) were kindly provided by Dr. Curzio Ruegg (University of Fribourg, Switzerland). Production and purification of the proteins were performed as described for the chimeric CARex-Fc (Ebbinghaus et al., 2001). Briefly,

about 10^7 COS cells were transiently transfected with 20 µg of each plasmid. Low FCS supernatant containing both proteins was adsorbed to protein G-Sepharose (Amersham Pharmacia). Following washing with PBS, bound protein was eluted using glycine-HCl (0.15 M, pH 2.8) and immediately neutralized with 1 M Tris pH 9.5. Eluted material was concentrated using centrifugal filter devices (Millipore, Bedford MA, USA), dialyzed against PBS and kept frozen in aliquots. The protein concentration of purified integrin-Fc was determined by BCA-assay and was 0.6 µg/µl. Protein yield was about 0.3 mg when transfecting 2 x 10^8 COS cells.

Biacore binding measurements of soluble αvβ3ex-Fc to Ad2

All experiments of SPR were performed on a Biacore T100 system (GE Healthcare) at 25°C with a CM3 sensor chip. All reagents including amine-coupling kit, HBS-P+ and CM3 chips were purchased from Biacore (GE Healthcare). HBS-N (10 mM Hepes, 150 mM NaCl, pH 7.4) plus 2 mM $MgCl_2$ was used as a running buffer for the measurement. The immobilization procedures included three steps. 1) activation of the surface by using 1:1 of 0.4 M 1-ethyl-3-(3-dimethylaminopropyl)-carbodiimide (EDC) in water and 0.1 M N-hydroxysuccinimide (NHS) in water for 420 seconds with flow rate of 5 µl/min, 2) immobilization of Ad2 to the chip in 10 mM sodium acetate pH 4.5, and 3) deactivation of excess reactive groups by 1 M ethanolamine-HCl pH 8.0 for 420 s with flow rate of 5 µl/min. The conditioning of the sensor chips with 50 mM NaOH was performed after immobilization. Next, the immobilization CM3 chip was serially tested with different concentration of analytes, CD46ex-Fc, CARex-Fc and αvβ3ex -FC in HBS-N buffer plus 2 mM $MgCl_2$ at a flow rate of 4 µl per min. After each cycle of binding, the chip surface was regenerated by injecting 3 M $MgCl_2$.

Cryo-section EM

Cryo-sections were prepared according to the Tokuyasu method (Slot and Geuze, 2007). Briefly, cells were fixed in 2% para-formaldehyde, 0.2% glutaraldehyde in 0.1 M cacodylate at room temperature for 60 min, collected by centrifugation at 800 x g into PBS-0.2% BSA, washed in PBS, resuspended in 10% gelatine at 37°C for 5 min, centrifuged at 12000 x g for 3 min, overlaid with fresh gelatine, and incubated for 1 h on ice. The gelled cell pellet was cut in small pieces and infiltrated with 2.3 M sucrose overnight. Cryo-sections were generated with a Leica-EM FCS (center for microscopy,

University of Zurich), rapidly collected from the knife onto sucrose / methylcellulose (2.3 M / 2% in H_2O) and transferred to parlodion EM specimen grids coated with carbon (135 mesh, Plano GmbH, Wetzlar, Germany). Cryo-sections were labeled with the rabbit polyclonal anti-fiber antibody R72 (Baum et al., 1972) at 0.01 mg/ml IgG fraction for 30 min in PBS containing goat serum, washed and stained with 0.2 µg/ml goat anti-rabbit IgG coupled to 10 nm colloidal gold (BBI International). Sections were stained by freshly prepared 1.8% methyl-cellulose containing 0.4% uranyl-acetate in H_2O for 20 to 30 s. The 2% methyl-cellulose was prepared as follows, and used immediately. 0.2 g of methylcellulose were suspended in 10 ml of double-quartz distilled H_2O, quick-heated in a microwave oven to 80-90°C, stirred at 80-90°C for 5 min, chilled in an ice-NaCl slurry and stirred for 30 min, which completely clarified the suspension. Images were recorded in a Zeiss TEM-10, typically at 50'000 magnification, 80 kV.

Fluorescence recovery after photobleaching (FRAP)

For FRAP, cells were imaged at 37°C on a Leica SP5 confocal laser scanning microscope (Leica Microsystems). GFP was excited using the 476 nm and 488 nm lines of an Ar laser, and emission was recorded in the range of 500 nm to 600 nm at a pinhole size of one airy disc and a pixel size of 0.13 µm. Bleaching was performed with the built in “FRAP wizard” at a laser power of 100%, while imaging was performed at 4% with a gain of 1000 and an offset of 0.5%. The imaging protocol was as follows. First, 10 images at maximal speed (1.3 s/frame), and then a region of 3x3 micrometers was bleached, followed by another 10 images at maximum speed. Afterwards 48 images were recorded in intervals of 5 s, and the series was finished by 10 images recorded at maximal speed. The recovery curves from several cells were averaged as follows: i) the background signal was measured in an unbleached region outside the cell and subtracted, and ii) the signal was normalized with the pre-bleach values obtained from the first 10 frames. The fluorescence recovery curves were fitted using least squares, and $T_{1/2}$ and recovery values were obtained thereof.

Supplemental References

Baum, S.G., Horwitz, M.S., and J.V. Maizel, J. (1972). Studies of the mechanism of enhancement of human adenovirus infection in monkey cells by simian virus 40. J Virol *10*, 211-219.

Ebbinghaus, C., Al-Jaibaji, A., Operschall, E., Schoeffel, A., Peter, I., Greber, U.F., and Hemmi, S. (2001). Functional and selective targeting of adenovirus to high affinity Fcg receptor I positive cells using a bispecific hybrid adaptor. J Virol *75*, 480-489.

Fender, P., Kidd, A.H., Brebant, R., Oberg, M., Drouet, E., and Chroboczek, J. (1995). Antigenic sites on the receptor-binding domain of human adenovirus type 2 fiber. Virology *214*, 110-117.

Greber, U.F., Willetts, M., Webster, P., and Helenius, A. (1993). Stepwise dismantling of adenovirus 2 during entry into cells. Cell *75*, 477-486.

Helmuth, J.A., Burckhardt, C.J., Koumoutsakos, P., Greber, U.F., and Sbalzarini, I.F. (2007). A novel supervised trajectory segmentation algorithm identifies distinct types of human adenovirus motion in host cells. J Struct Biol *159*, 347-358.

Hilgendorf, A., Lindberg, J., Ruzsics, Z., Honing, S., Elsing, A., Lofqvist, M., Engelmann, H., and Burgert, H.G. (2003). Two distinct transport motifs in the adenovirus E3/10.4-14.5 proteins act in concert to down-modulate apoptosis receptors and the epidermal growth factor receptor. J Biol Chem *278*, 51872-51884.

Imelli, N., Ruzsics, Z., Puntener, D., Gastaldelli, M., and Greber, U.F. (2009). Genetic reconstitution of the human adenovirus type 2 temperature-sensitive 1 mutant defective in endosomal escape. Virol J *6*, 174.

Nakano, M.Y., Boucke, K., Suomalainen, M., Stidwill, R.P., and Greber, U.F. (2000). The first step of adenovirus type 2 disassembly occurs at the cell surface, independently of endocytosis and escape to the cytosol. J Virol *74*, 7085-7095.

Puntener, D., Engelke, M.F., Ruzsics, Z., Strunze, S., Wilhelm, C., and Greber, U.F. (2011). Stepwise loss of fluorescent core protein V from human adenovirus during entry into cells. J Virol *85*, 481-496.

Sakamoto, T., Limouze, J., Combs, C.A., Straight, A.F., and Sellers, J.R. (2005). Blebbistatin, a myosin II inhibitor, is photoinactivated by blue light. Biochemistry *44*, 584-588.

Sbalzarini, I.F., and Koumoutsakos, P. (2005). Feature point tracking and trajectory analysis for video imaging in cell biology. J Struct Biol *151*, 182-195.

Sirena, D., Lilienfeld, B., Eisenhut, M., Kaelin, S., Boucke, K., Beerli, R.R., Vogt, L., Ruedl, C., Bachmann, M.F., Greber, U.F*., et al.* (2004). The human membrane cofactor CD46 is a receptor for species B Adenovirus serotype 3. J Virol *78*, 4454-4462.

Sjoback, R., Nygren, J., and Kubista, M. (1988). Characterization of fluoresceinoligonucleotide conjugates and measurement of local electrostatic potential. Biopolymers *46*, 445-453.

Slot, J.W., and Geuze, H.J. (2007). Cryosectioning and immunolabeling. Nat Protoc *2*, 2480-2491.

Studier, F.W. (2005). Protein production by auto-induction in high density shaking cultures. Protein Expr Purif *41*, 207-234.

Suomalainen, M., Nakano, M.Y., Boucke, K., Keller, S., Stidwill, R.P., and Greber, U.F. (1999). Microtubule-dependent minus and plus end-directed motilities are competing processes for nuclear targeting of adenovirus. J Cell Biol *144*, 657-672.

Volpers, C., and Kochanek, S. (2004). Adenoviral vectors for gene transfer and therapy. J Gene Med *6 Suppl 1*, S164-171.

Zacharias, D.A., Violin, J.D., Newton, A.C., and Tsien, R.Y. (2002). Partitioning of lipid-modified monomeric GFPs into membrane microdomains of live cells. Science *296*, 913-916.